

Computational modeling of food extrusion systems for optimal plant-based meat production

by

Gregory Gause

B.S., United States Military Academy, 2011

A REPORT

submitted in partial fulfillment of the requirements for the degree

MASTER OF SCIENCE

Department of Chemical Engineering
Carl R. Ice College of Engineering

KANSAS STATE UNIVERSITY
Manhattan, Kansas

2023

Approved by:

Major Professor
Dr. Davood Pourkargar

Copyright

© Gregory Gause 2023.

Abstract

In recent years, consumers have had growing interest in non-meat alternative food sources to mimic the feel, texture, and taste of meat without the adverse side effects of high cholesterol, the resources needed to raise livestock, and the ethical concerns around the treatment of animals. Pea and plant proteins have been one of the main focuses of research into meat substitutes since they are not genetically modified and have low allergenic properties. A significant obstacle in processing plant proteins lies in the extrusion process. Food extrusion consists of introducing mixing, heating, and shear stress conditions to a food material inside a tank and then forcing this food material through a die. The material then expands upon exiting the die to form its final shape and consistency. The effects of heat and mass transfer play a significant role in the overall quality of the final product. This review will focus on the extrusion process, its effects on texture, taste, moisture content, and other material properties and avenues to improve this process. It will also use the extrusion process of polymers to better understand the heat and mass transfer phenomena involved in extrusion. Finally, we will discuss modeling tools available to establish predictions of the extrusion process to ultimately create our own model.

Table of Contents

List of Figures	v
List of Equations	vi
List of Tables	x
Introduction.....	1
Review of the Literature	3
Methodology.....	29
Results.....	50
Discussion	53
Conclusion	55
References.....	56

List of Figures

Figure 1: Chemical Structure of Saturated Fat (Above) and Unsaturated Fat (below) ⁵⁴	2
Figure 2: Partitioned Modeling Sections of Extruder ²⁰	25
Figure 3: Common Extruder Schematics ³⁹	34
Figure 4 : Pressure Field	50
Figure 5: Temperature Field	51
Figure 6: yz Plane of Temperature Field	51
Figure 7: xy Plane of Velocity Field.....	52
Figure 8: yz Plane of Velocity Field.....	52

List of Equations

Equation 1: Polynomial Regression Equation ⁵	4
Equation 2: Momentum Governing Equation ⁸	6
Equation 3: Melt Flow Rate Solution ⁸	6
Equation 4: Pressure to Drag Flow Relationship ⁸	7
Equation 5: Stress Terms Based on Screw Geometry ⁸	7
Equation 6: Shear Stress Based on Irregular Shaped Die ⁸	7
Equation 7: Weighted Average Total Strain ⁸	7
Equation 8: One-dimensional Heat Transfer ⁸	8
Equation 9: Nusselt Number Based on Geometry ⁸	8
Equation 10: Nusselt Number Based on Screw Diameter and Viscosity ⁸	8
Equation 11: Heat Transfer Assuming No Heat Transfer to Screw Shaft ⁸	8
Equation 12: Temperature Profile of Melt ⁸	9
Equation 13: Energy Balance Melt Pumping Section ⁸	9
Equation 14: Constants for Energy Balance ⁸	9
Equation 15: Constant for Melt Pumping Section ⁸	9
Equation 16: Three-dimensional Fluid Flow Governing Equations ⁹	10
Equation 17: Boundary Conditions for Screw Velocity Profiles ⁹	10
Equation 18: Finite Difference Method Discretized Equation ⁹	10
Equation 19: Modified Hershel-Bulkley Equation to Model Viscosity ¹⁰	11
Equation 20: Momentum and Velocity Distribution Governing Equations ¹⁰	11
Equation 21: Residence Time Distribution ¹⁰	11
Equation 22: Governing Equation of Momentum with No Pressure Gradient in Conveying Section ¹¹	12
Equation 23: Equation of Flow Through the Extruder Die ¹¹	12
Equation 24: Power Law Viscosity Equation ¹¹	12
Equation 25: Shear Rate in Intermeshing Twin Screw Extruder ¹¹	12
Equation 26: Heat Transfer Mechanisms with Moving Interface ¹¹	13
Equation 27: Viscous Heat Generation Rate ¹¹	13

Equation 28: Boundary Conditions for Heat Transfer with Moving Interface ¹¹	13
Equation 29: Ostwald-de Waele Power Law for Viscosity ¹²	13
Equation 30: Pressure Development Neglecting Leakage Flow ¹²	14
Equation 31: Drag and Pressure Flow Correcting Shape Factors ¹²	14
Equation 32: Elastic and Yield Stress ¹²	14
Equation 33: Rate of Change of Bubble Radius ¹²	15
Equation 34: Bubble Shrinkage Rate ¹²	15
Equation 35: Expansion Ratio (Macroscopic and Microscopic Parameters) ¹²	15
Equation 36: Volumetric Flow Rate Through Screw Channel ¹³	16
Equation 37: Energy Balance and Power Dissipation Through Screw Channel ¹³	16
Equation 38: Melt Consistency and Flow Index ¹³	16
Equation 39: Bulk Density ¹⁴	17
Equation 40: Viscosity Model Equation Based on SME ¹⁴	17
Equation 41: Buckingham Pi Dimensional Analysis of Extrusion ¹⁵	18
Equation 42: Bulk Density Equation – Buckingham Pi Analysis ¹⁵	18
Equation 43: Bulk Density with Shear Term Added ¹⁵	18
Equation 44: Pressure Difference During Bubbling ¹⁶	19
Equation 45: Radius Change During Bubbling ¹⁶	19
Equation 46: Moisture Diffusion Governing Equation with Boundary Conditions ¹⁶	19
Equation 47: Number of Open Bubbles During Extrusion ¹⁶	19
Equation 48: Momentum Governing Equation Incorporating Bubbling ¹⁶	19
Equation 49: Boundary Conditions for Momentum Equation ¹⁶	20
Equation 50: Moisture Diffusion in the Extrudate ¹⁶	20
Equation 51: Heat Transfer Governing Equation (Fourier’s Law) ¹⁶	20
Equation 52: Boundary Conditions for Heat Transfer ¹⁶	21
Equation 53: Bubble Growth for a Single Bubble ¹⁷	21
Equation 54: Bubble Growth for Multiple Bubbles ¹⁷	22
Equation 55: Generalized Form of Darcy’s Equation ¹⁸	23
Equation 56: Darcy Equation for Velocity ¹⁸	23
Equation 57: Energy Balance of Extrusion with Convection, Conduction, and Phase Change ¹⁸ 23	
Equation 58: Momentum Balance with Phase Change ¹⁸	23

Equation 59: Nusselt Number for Axial Convection Through a Cylinder ¹⁸	24
Equation 60: Specific Mechanical Energy (SME) ¹⁸	24
Equation 61: Shear Stress Incorporating Screw Geometry ¹⁹	24
Equation 62: Apparent Viscosity ¹⁹	24
Equation 63: Shear Stress With Slip Conditions at Walls ²³	25
Equation 64: Shear Rate of Melt Flow with Viscoelastic Effects ⁵¹	27
Equation 65: Heat Transfer in Large Extruders with High Peclet Number ⁵¹	27
Equation 66: Pressure Gradient in Twin Screw Extruder ⁵²	27
Equation 67: Modified Pressure Equation Incorporating Carreau Model ⁵²	27
Equation 68: Governing Equation of Momentum ¹⁶	39
Equation 69: Continuity Equation for Pressure Gradient ¹⁶	39
Equation 70: Velocity Term ¹¹	39
Equation 71: Shear Rate in Screw Section ¹¹	40
Equation 72: Shear Rate in Die Section ¹¹	40
Equation 73: Pressure Differential ¹⁶	40
Equation 74: Failure Stress ¹⁶	41
Equation 75: Shear Stress ⁸	41
Equation 76: Specific Heat Capacity of the Melt ³³	42
Equation 77: Thermal Conductivity of the Melt ³³	42
Equation 78: Nusselt Number Equations ¹⁹	42
Equation 79: Rayleigh Number ¹⁹	42
Equation 80: Prandtl Number ¹⁹	42
Equation 81: Gas Permeability ¹⁹	43
Equation 82: Governing Equation of Heat Transfer in Melt ¹¹	43
Equation 83: Heat Flux at the Surface ¹¹	43
Equation 84: Power Law Fluid Viscosity Equation ¹⁶	44
Equation 85: Consistency and Flow Index ¹³	44
Equation 86: Specific Mechanical Energy ¹⁴	44
Equation 87: Expansion Ratio ¹²	46
Equation 88: Bulk Density of the Melt ¹⁵	47
Equation 89: Diffusion of Water Vapor into Melt Bubbles ¹⁶	47

Equation 90: Mass Flow Rate ¹⁶	48
Equation 91: Diffusion of Water in the Extrudate ¹⁶	48
Equation 92: Inner Vapor Generation Rate ¹⁶	48

List of Tables

Table 1: Operating Ranges for Computational Model.....	38
--	----

Introduction

Growing Importance of Plant-Based Meat Alternatives

There have been significant changes in the consumer demand for plant-based meat alternatives in recent years. A section of the consumer base has significant ethical concerns when it comes to livestock production. Meat production also takes up approximately 83% of arable land worldwide, consumes 36% of the earth's food and water, and generates between 17-34% of all CO₂ emissions ²⁷. In addition, the plant-based meat market is estimated to reach a market cap of \$15 billion by 2026²⁸. Meat eating is also associated with higher cholesterol levels and health problems. The push for more organic-based products that are better for the environment has created a new avenue for exploring plant-based meat alternatives. The issue at hand is mimicking the popular qualities of meat in plant-based alternatives, which has had mixed success until now. Plant-based meat products, primarily soy, pea proteins and wheat gluten, are processed in an extrusion cooker. Subjected to high heat and stress within the extruder, the overall makeup of the product at hand undergoes significant changes. The goal of any plant-based meat extrusion process is to change the fibrous structure of the plant protein into that of a meat-like structure by rearranging molecular particles, altering fats, and trapping water to form a new fibrous structure²⁷. Plant protein bases with good gelation properties are more conducive to this process as they can more easily obtain a mesh-like structure akin to meat²⁷. As the extrusion melt (plant protein) is subjected to extreme conditions during the cooking process, their proteins are unfolded and cross-linked, creating a layer and fiber structure²⁸. This process aims to get this structure as close as possible to meat proteins, as meat proteins have muscle fibers with an interstitial matrix conducive to water binding²⁸. This is what gives meat its taste and texture. The cell structure of the extruded plant-based meats also affects oil uptake, which is essential for cooking techniques after the extrusion process, like frying¹².

A major challenge to replicating the meat taste is mimicking animal fats. Fats give animal meat a tender flavor and are highly hydrophobic. Animal fats contain largely saturated fats which are unhealthier than the unsaturated fat commonly found in plant-based meats. Saturated fats are typically straight, single bonded carbon chains composed in a collagen fiber network. Plant-

based meat unsaturated fats have double and sometimes triple bonded carbons, which gives their structures a more crooked orientation. This composition leads to animal fats being solid at room temperature, while most plant-based fats are liquid⁵³. One objective of plant-based meat production is to unfold and cross link the chemical structures of unsaturated fats to align more closely with that of saturated fats to better mimic taste.

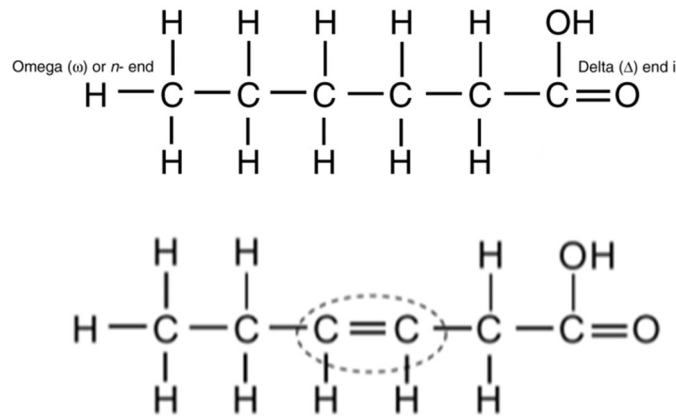


Figure 1: Chemical Structure of Saturated Fat (Above) and Unsaturated Fat (below)⁵⁴

This project will focus on creating a mathematical modeling framework to simulate the food extrusion cooking process for plant-based meat products. To create the model, we must determine the critical parameters we will attempt to model. These parameters would be the key factors that either enhance or detract from the taste, texture, color and “feel” of plant proteins used as meat substitutes to mimic the meat-eating experience. Nine properties will be modeled: momentum, shear rate, shear stress, heat transfer, viscosity, specific mechanical energy, expansion ratio, bulk density, and diffusion (moisture content).

Review of the Literature

Martinez et al. discussed the challenges of mimicking meat using chickpea products. They discussed how the functional properties of proteins are the main drivers in establishing a “meat” feel and taste. These include protein solubility, emulsification, foaming, gelation behavior, water, and fat absorption¹. Extrusion is identified as a simple and cost-effective method for producing legume-based foods. It is noted that the moisture content of the feed, feed rate, screw speed, and temperature within the barrel are the primary parameters that effect the extrusion process and desired product. A high feed rate led to more gelatinization due to thermal energy, while a high screw speed resulted in lower viscosity¹. Factors that need investigation when optimizing the extrusion process included bulk density, water absorption index, solubility index, and hardness. High protein concentrations are also noted to raise the hardness within chickpeas, which is a generally undesirable by-product, commercially speaking, to come out of extrusion. Additives to improve the extrusion process are also discussed, showing that stabilizers and soluble fibers can be used to improve texture¹.

Angelova et al. pointed to a high expansion ratio, a low bulk density, and a firm texture as sought-after properties at the end of an extrusion process. Their study focused on the effects of ingredient properties and conditions within an extruder on the end-state quality of the finished product. They defined the section expansion index (SEL) as the ratio of the diameter of the extrudate to the diameter of the die². This team used a regression model with a linear and quadratic term to predict the expansion index based on various parameters, including moisture content, extrusion barrel temperature, and screw speed. They also detailed the corresponding bulk densities. It is determined that screw speed has the most considerable effect on the expansion index. They also determined that feed moisture content and barrel temperature have the highest effect on bulk density². As moisture content increased, associated temperature increases began to lower expansion due to a decrease in viscosity. They also pointed out that insufficient water for vaporization at high temperatures can lead to high bulk density values². Meng et al. took a similar approach to Angelova by using a second-order polynomial regression model to predict end-product properties in an extrusion process. They used a canonical analysis to find the ideal extrusion system parameters, leading to a minimum density, hardness, and maximum expansion ratio. Their models also used three independent variables: screw speed,

moisture content, and barrel temperature. Finally, the model used linear, quadratic, and interaction effects of these variables to establish a regression analysis for predicted results³.

$$y_i = b_o + \sum_{i=1}^3 (b_i X_i) + \sum_{i=1}^3 \left(\sum_{j=1}^3 (b_{ij} X_i X_j) \right)$$

Equation 1: Polynomial Regression Equation⁵

Product temperature decreased with increased moisture content since more moisture reduced the viscosity and mechanical energy dissipation within the extruder, while higher screw speed generated more mechanical energy, leading to higher internal temperatures³. It is also determined that die pressure reduced with higher moisture content, possibly due to lower viscosity. Screw speed influenced die pressure at low temperatures but not nearly as much at higher temperatures. The authors produced a response surface plot and showed that an increase in screw speed resulted in a significant increase in expansion ratio at low moisture content levels but had a negligible effect at high moisture content levels. Barrel temperature had a quadratic effect on the expansion ratio with a plateau between 150 and 170 degrees Celsius³. Bulk density and hardness effects were also discussed in detail.

Guldiken et al. used response surface methodology (RSM) to evaluate the conditions of the extrusion process and how they affect the physical properties of chickpeas in a 60:40 chickpea barley blend. Here, barrel temperature and moisture content were independent variables⁴. Response parameters were discussed and analyzed, including hardness, expansion index, bulk density, and protein quality. They found that the expansion index is increased with higher moisture content and lower barrel temperature. At low temperatures, there was reduced protein denaturation, which increased the ability of the product to expand when it exits the die. Hardness had a greater variability with moisture content at lower temperatures and became less variable at higher temperatures with respect to moisture content⁴. Empirical equations were used to describe the relations for expansion index, bulk density, and hardness based on moisture content and barrel temperature. They found that the ideal properties of high expansion, low bulk density, and low hardness are achieved at high barrel temperatures and high moisture content⁴.

Manepalli et al. used a Monte Carlo analysis to determine the variability within an extrusion cooking process of degermed corn meal. The analysis was broken down into four key

components: variability of input parameters, the sampling of the variability of input, implementation of the model, and the analysis of the result⁵. Sensitivity analysis was then conducted on input parameters, including moisture content, screw speed, and a consistency index coefficient. Data acquisition systems were used to measure water content and screw speed during extrusion⁵. From this data, the standard deviation and the mean were determined, thereby obtaining the coefficient of variation. The authors then used random sampling to get inputs into their model and achieved test results. Bubble shrinkage was explained in detail, showing that as the material left the extruder (die), bubbles grew due to the high cell wall thickness of the bubble⁵. The temperature then dropped after leaving the die, which caused a decrease in vapor pressure inside the bubble and resulted in the shrinkage of the bubble. When die temperatures decreased, vapor pressure decreased, reducing the expansion ratio. This process was reversed for high temperatures. It was also shown that an increase in moisture content reduced melt elasticity and led to a reduced expansion ratio⁵.

Webb et al. noted that a larger starch content resulted in higher viscosity within an extruder, which created more mechanical energy and shear in the process⁶. Mechanical energy led to greater texturization in pea-based proteins but adding too much starch led to higher moisture content through expansion. Too much expansion is generally unfavorable in the extrusion process, so a delicate balance ensues. They noted that more moisture would, in theory, act as a plasticizer and reduce mechanical energy in the extruder⁶. However, with no starch added to a pea-based protein, more moisture increased mechanical energy as the high protein content resulted in greater texturization and more resistance to flow in the extruder. The mechanical energy then increased after a certain threshold of starch is added, as there is a competing effect between gelatinization and protein texturization⁶. Starch created viscosity which increased mechanical energy. Starch gelatinization eventually prevented protein texturization, and more starch-protein interactions occurred. This led to products with higher porosity and expansion. Bulk density generally decreased as more starch is added due to higher expansion from starch gelatinization. Moisture content generally increased with more starch. The authors also noted that water content plays a significant role in the “meat-like” texture, and most meat products have between 55-75% moisture. High starch contents led to more “chewiness” due to gelatinization and fewer protein-protein interactions⁶.

Gu et al. gave a comprehensive overview of the extrusion process. The extrusion process consists of a screw or set of screws that push food products through a small opening. During this process, food is contained in a barrel and is subjected to high pressure, shear, and temperature to cook it. These external forces that act upon the food material turn it from a solid state to a melted state when in the extruder barrel⁷. Once the food material exits through an opening (called a die), it expands through the pressure drop that occurs as well as the process of converting water into steam. Steam forms small pockets within the material that exits the die and expands, which causes the product to also expand in all directions. Extrusion is generally cheap and can consist of single or double-screw systems. It also has the ability for mass production of food in an easily repeatable process. The extruder consists of a feeder that pushes the food material into a barrel containing screws. Barrels can be insulated, heated, or have injection ports for materials or water. The screw inputs shear into the material, creates pressure within the barrel, and ultimately pushes the food material through the die and out of the extruder. The die is used to control the shape and size of the final product⁷.

Kumar et al. explained how to model engineering principles within an extruder. They stressed the importance of modeling fluid flow in an extruder which can give us insight into Residence Time Distribution, mixing mechanisms, flow rate predictions, pressure changes, and energy modeling. Flow within an extruder was assumed to be non-Newtonian and non-isothermal. They stated flow can be modeled using the momentum transfer equation of:

$$\frac{1}{\mu} \left(\frac{\delta P}{\delta z} \right) = \left[\frac{\delta^2 v_z}{\delta x^2} + \frac{\delta^2 v_z}{\delta y^2} \right]$$

Equation 2: Momentum Governing Equation⁸

This assumed a steady state, laminar flow with no-slip boundary conditions, no curvature along the barrel, and no viscous, gravitational, or inertial forces⁸. This equation was solved to yield a solution for the flow rate, with p representing the number of channels present (2 for double screw extruders).

$$Q = p \frac{V_z WH}{2} F_d + p \frac{WH^3}{12\mu} \left(\frac{\delta P}{\delta z} \right) F_p = Q_d + Q_p$$

Equation 3: Melt Flow Rate Solution⁸

Q_d represents the drag flow while Q_p represents the pressure flow⁸. The relationship of pressure to drag flow is given by

$$a = \frac{Q_p}{Q_d} = \frac{H^2}{6V_z\mu} \frac{\delta P}{\delta z} \frac{F_p}{F_d}$$

Equation 4: Pressure to Drag Flow Relationship⁸

with F_p and F_d representing the shape factors due to pressure and drag, respectively. By solving for the velocity in the x direction, the authors concluded that the cross-channel velocity is not affected by the downward pressure gradient⁸. It is noted that there is a third type of flow due to leakage. This is due to the gap between the screw and the barrel within an extruder. This model assumed isothermal conditions, which may not be practical in an actual extrusion process⁸. For non-Newtonian fluids, pressure drop across the die was determined from the below equations, which depend on the geometry of the die.

$$\gamma = \frac{3n+1}{4n} \frac{4Q}{\pi R^3}, \tau = \frac{R\Delta P}{2L_d} \text{ (circular)}$$

$$\gamma = \frac{2n+1}{3n} \frac{3Q}{2C^2W}, \tau = \frac{C\Delta P}{L_d} \text{ (slit)}$$

Equation 5: Stress Terms Based on Screw Geometry⁸

Here, τ is the effective shear stress at the wall, and L and R are the lengths and radius, respectively. If the shape of the die is irregular, one must use the hydraulic radius, determined from the cross-sectional area and wetted perimeter of the die⁸.

$$\tau = \frac{\Delta P}{2\left(\frac{L}{R} + \frac{L'}{R}\right)}$$

Equation 6: Shear Stress Based on Irregular Shaped Die⁸

The authors also noted the importance of modeling mixing within an extruder. The weighted average total strain (WATS) describes the level of deformation a product goes through in the extrusion process, which is an indicator of the level of mixing⁸. This was determined by the below equation, where γ represents the shear strain.

$$\gamma = \int_0^{\infty} \gamma E(t) dt$$

Equation 7: Weighted Average Total Strain⁸

Heat transfer is also critical to model the extrusion process to control cooking. The authors detailed two ways to model heat transfer. The first involved an energy balance of the process using different types of power. The second revolved around heat transfer within the extruder barrel. The one-dimensional heat transfer equation was given by

$$dH = dq + h_{m/b} dS_{m/b} (T_b - T_m) + h_{m/s} dS_{m/s} (T_s - T_m)$$

Equation 8: One-dimensional Heat Transfer⁸

dH represents the change in internal energy, dq is the heat added to the process (positive if there is viscous dissipation present and negative when there is an endothermic reaction in the barrel), $h_{m/b}$ is the convective heat transfer coefficient between the food material and the barrel, $h_{m/s}$ is the heat transfer coefficient between material and screw and dS represents the surface area for heat transfer⁸. Heat transfer coefficients were determined from the Nusselt number, which was based on the geometry of the extruder and is shown below (K_1 and K_2 are empirical parameters)⁸.

$$Nu = \frac{hD}{k} = \left(\frac{PeH}{L}\right)^{K_1} Br^{K_2}$$

Equation 9: Nusselt Number Based on Geometry⁸

The Nusselt number was also determined using the screw diameter and viscosity of water for single screw extruders⁸.

$$Nu = \frac{hD_{ext}}{K} = 0.94 \left(\frac{D_{ext}^2 N \rho}{\mu}\right)^{0.28} Pr^{.33} \left(\frac{\mu}{\mu_w}\right)^{0.14}$$

Equation 10: Nusselt Number Based on Screw Diameter and Viscosity⁸

An energy balance equation that incorporates non-Newtonian, non-isothermal parameters with the laminar flow at a steady state while assuming no heat transfer to the screw shaft was used and is shown below

$$m_s c_{ps} T + FU_s A (T_b - T) \delta x = m_s c_{ps} (T + dT)$$

Equation 11: Heat Transfer Assuming No Heat Transfer to Screw Shaft⁸

Here F is the degree of fill, U is a heat transfer coefficient that incorporates both conduction and convection, and A is the surface area⁸. The authors established a boundary condition of $T_{x=0} = T_o$, and solved for a temperature profile equation

$$T = T_b - (T_b - T_f) \exp\left(\frac{-F U A x}{m_s c_p}\right)$$

Equation 12: Temperature Profile of Melt⁸

They modeled the extrusion process based on the melt pumping section and the melt shearing section⁸. The solid material changed to a fluid melt in the pumping section, and the screw filled. The melt pumping section energy balance was described as

$$\frac{\delta T}{\delta x} = C_{2p} \exp(-b_1 T) + C_{3p} (T_b - T)$$

Equation 13: Energy Balance Melt Pumping Section⁸

With $C_{2,p}$ and $C_{3,p}$ were constants represented by

$$C_{2,p} = \frac{C_{1p} \mu N^2}{\pi D (\tan\theta) m_s c_p}, C_{3,p} = \frac{F A}{m_s c_p}$$

Equation 14: Constants for Energy Balance⁸

The melt shearing section incorporated cross channels, and the temperature profile was expressed similarly as the melt pumping section, with a new constant of $C_{4,s}$ introduced to the equation

$$C_{4s} = \frac{m D \mu \gamma \left(1 - \frac{m B G}{\pi D H}\right)}{c_p H^5 (\tan\theta)}$$

Equation 15: Constant for Melt Pumping Section⁸

Ferretti and Montanari developed a finite difference model to account for geometry in the extrusion process as well as defects and flow instabilities. A well-controlled velocity field can improve the overall quality of the extrusion process. However, a consistent shear profile with a low value across the extruder can reduce gelatinization, and high values of mean shear rate can be detrimental to the quality control of the product⁹. Their study incorporated a single, rotating

screw extruder with a stationary barrel. They assumed laminar flow due to generally high viscosities of extruded material, neglected the inertia term of the Navier-Stokes equation since the viscous and pressure terms are more pronounced, neglected gravitational force, and assumed an incompressible, Newtonian fluid with the fully developed flow with no-slip boundary conditions⁹. Three-dimensional fluid motion was expressed as follows:

$$\begin{aligned}\frac{\delta P}{\delta x} &= \mu \left(\frac{\delta^2 V_x}{\delta y^2} + \frac{\delta^2 V_x}{\delta z^2} \right) \quad \text{x-component} \\ \frac{\delta P}{\delta y} &= \mu \left(\frac{\delta^2 V_y}{\delta y^2} + \frac{\delta^2 V_y}{\delta z^2} \right) \quad \text{y-component} \\ \frac{\delta P}{\delta z} &= \mu \left(\frac{\delta^2 V_z}{\delta y^2} + \frac{\delta^2 V_z}{\delta z^2} \right) \quad \text{z-component}\end{aligned}$$

Equation 16: Three-dimensional Fluid Flow Governing Equations⁹

The velocity term in the y direction was neglected for screws with a small depth-to-width ratio⁹. Since screw velocities are a function of the radius and are not constant, boundary conditions for the x-component were expressed as

$$\begin{aligned}V_x(z, H) &= 0 \quad (\text{barrel}) \\ V_x(0, y) &= \omega R_s \cos(\theta) \quad (\text{screw root}) \\ V_x(0, y) &= \omega (R_s + y) \cos(\theta) \quad (\text{screw root}) \\ V_x(W, y) &= \omega (R_s + y) \cos(\theta) \quad (\text{screw flights})\end{aligned}$$

Equation 17: Boundary Conditions for Screw Velocity Profiles⁹

The authors then discretized the domain of their equation in the x direction. Finally, they employed the finite difference method using excel to solve for the velocity term. A mesh plot can then be implemented, showing the velocity gradient across the barrel⁹.

$$V_x(i, j) = \frac{h_y^2 h_z^2}{2 (h_y^2 + h_z^2)} \left[\frac{V_x(i+1, j) + V_x(i-1, j)}{h_y^2} + \frac{V_x(i, j+1) + V_x(i, j-1)}{h_z^2} - \frac{1}{\mu} \frac{\delta P}{\delta x} \right]$$

Equation 18: Finite Difference Method Discretized Equation⁹

Dhanasekharan and Kokini delved into the area of extrusion scaling. They determined that flow and power requirements are related by an x^3 factor to the dimensions of an extruder.

Additionally, heat transfer elements and viscous dissipation of mechanical energy increased by a factor of x^2 to dimensions since they have a relationship to surface area¹⁰. The authors used

wheat dough as their basis, which is dominated by shear forces within the metering section of an extruder. To model viscosity, a modified form of the Hershel-Bulkley equation was used¹⁰.

$$\eta (\gamma, T, MC, \varphi, \phi) = [K\gamma^{n-1} + \frac{\tau_0}{\gamma}] [\exp(\frac{\alpha}{T} - \frac{\alpha}{T_0})] x [\exp \{b (MC - MC_r)\}] [A' \{1 - \exp(-k_a \varphi)\}^a] [1 - \beta \{1 - \exp(-d\phi)\}]$$

Equation 19: Modified Hershel-Bulkley Equation to Model Viscosity¹⁰

The study defined specific mechanical energy as the amount of mechanical energy dissipated via heat per unit mass of the material. It is equal to the input of work from the motor of the extruder¹⁰. The governing equations used for the momentum balance and velocity distribution are:

$$\begin{aligned} -\nabla P + \nabla \tau &= 0 \\ \tau &= \eta (\nabla V + \nabla V^T) \\ \rho C_p (V \nabla T) - \tau \nabla V + \nabla q &= 0 \end{aligned}$$

Equation 20: Momentum and Velocity Distribution Governing Equations¹⁰

They also considered Residence Time Distribution in their model, which was defined as:

$$\int_0^{\infty} E(t) dt = 1$$

Equation 21: Residence Time Distribution¹⁰

It is noted that food materials have a very small thermal diffusivity (10^{-5} to $10^{-8} \frac{m^2}{s}$). This results in a very large Peclet number, which gives utmost significance to the convective heat transport in the extrusion process¹⁰. They showed in their numerical model that increasing screw diameter while keeping channel depth constant increased the specific mechanical energy, reducing the depth of the channel which resulted in higher shear rates due to a bigger velocity gradient. They also noted an increase in the helix angle of the screw reduced specific mechanical energy due to the reduction in the number of turns the screw makes¹⁰.

Wang et al. developed a model to predict fluid flow, heat transfer, and melting kinetics for a starch material in a twin screw, intermeshing extruder, using transport phenomena equations and a finite element scheme to solve. Two types of flow exist in the extrusion process: plug flow in the conveying section and non-Newtonian melt flow in the die channel¹¹. The authors assumed

the screw is stationary, that there is no pressure gradient in the conveying section, and that the process has a laminar, fully developed flow with no-slip boundary conditions. They also neglected the gravitational and inertia components of the Navier-Stokes equation and the diffusion of momentum in the z direction¹¹. The governing equations used for momentum were

$$\begin{aligned}\frac{\delta P}{\delta x} &= \frac{\delta}{\delta y} \left(\eta \frac{\delta u_x}{\delta y} \right) \quad \text{x-component} \\ \frac{\delta P}{\delta y} &= 0 \quad \text{y-component} \\ \frac{\delta P}{\delta z} &= \frac{\delta}{\delta x} \left(\eta \frac{\delta u_z}{\delta x} \right) + \frac{\delta}{\delta y} \left(\eta \frac{\delta u_z}{\delta y} \right) \quad \text{z-component}\end{aligned}$$

Equation 22: Governing Equation of Momentum with No Pressure Gradient in Conveying Section¹¹

To model flow through the die, they assumed isothermal, non-Newtonian conditions, and a symmetrical die¹¹. This led to a governing equation of momentum as

$$\frac{\delta P}{\delta z} = \frac{1}{r} \frac{\delta}{\delta r} \left(\eta r \frac{\delta u_z}{\delta r} \right)$$

Equation 23: Equation of Flow Through the Extruder Die¹¹

With a boundary condition of $\frac{\delta u_z}{\delta r} \Big|_{r=0} = 0$ and $\mu_z \Big|_{r=R} = 0$ ¹¹. Viscosity was calculated assuming it follows the power law.

$$\eta = 106.25 \gamma^{-0.63} \exp\left(\frac{2451}{T_k}\right) \exp(-4.63 X_w)$$

Equation 24: Power Law Viscosity Equation¹¹

With the shear rate determined through the following equations

$$\begin{aligned}\gamma &= \left[\left(\frac{\delta u_x}{\delta y} \right)^2 + \left(\frac{\delta u_z}{\delta x} \right)^2 + \left(\frac{\delta u_z}{\delta y} \right)^2 \right] \quad (\text{Screw Channel}) \\ \gamma &= \frac{\delta u_z}{\delta r} \quad (\text{Die Channel})\end{aligned}$$

Equation 25: Shear Rate in Intermeshing Twin Screw Extruder¹¹

While developing their model for heat transfer, the authors noted that solid material begins to model non-Newtonian fluid flow once starch conversion reaches approximately 37 percent¹¹. They assumed a uniform distribution of the convective heat transfer from the barrel and the

viscous dissipation to the melt. They divided their heat transfer analysis into two sections, separated by a moving interface during the melting process¹¹. Heat transfer through the solid portion was represented by

$$\rho_s c_s \frac{dT_s}{dt} = \frac{1}{r^2} \frac{\delta}{\delta r} (r^2 k_s \frac{dT_s}{dr}) \quad (\text{Solid Portion of Melting Process})$$

$$\rho_m c_m \frac{dT_m}{dt} = \frac{1}{r^2} \frac{\delta}{\delta r} (r^2 k_m \frac{dT_m}{dr}) = q_m \quad (\text{Melt Portion of Melting Process})$$

Equation 26: Heat Transfer Mechanisms with Moving Interface¹¹

Viscous heat generation rate, q_m , was defined as

$$q_m = \eta \dot{\gamma}^2$$

Equation 27: Viscous Heat Generation Rate¹¹

The boundary conditions used in this model are expressed below, with q_s being the heat flux on the particle surface

$$\left. \frac{\delta T_s}{\delta r} \right|_{r=0} = 0$$

$$T_s \Big|_{r=R_s} = T_m \Big|_{r=R_s} = T_{m0}$$

$$k \left. \frac{\delta T}{\delta r} \right|_{r=R_p} = q_{sur}$$

Equation 28: Boundary Conditions for Heat Transfer with Moving Interface¹¹

They were able to determine that heat transfer in small particles is dominated by convection between the barrel and material, while heat transfer in larger particles is driven by both convection and conduction within a particle¹¹.

Manepalli et al. investigated flow behavior and bubble growth within an extruder using starchy melts. The authors noted that modeling polymers in an extruder is much easier compared to food products due to the uniformity in the structure of polymers¹². They modeled the viscosity of the melt by the Ostwald-de Waele power law formula

$$\eta = K \dot{\gamma}^{n-1}$$

Equation 29: Ostwald-de Waele Power Law for Viscosity¹²

They calculated pressure developed within the extrusion process by neglecting leakage flow and focusing on drag flow and pressure flow as the only two components of pressure development¹².

$$\frac{Q_v}{lv} = F_D 0.25 N D^2 \cos(\theta) \left[1 - \left(\frac{D^2}{D^2 - D_i^2} \right) \ln \left(\frac{D}{D_i} \right)^2 \right] \left(1 - \frac{n_{fe}}{t} \right) - F_P \frac{1}{32\mu} \frac{\Delta P_e}{\Delta \theta} (D^2 - D_i^2) \left(1 - \left(\frac{2DD_i}{D^2 - D_i^2} \ln \left(\frac{D}{D_i} \right)^2 \right) \left(\frac{n_{fe}}{t} \right) \right)$$

Equation 30: Pressure Development Neglecting Leakage Flow¹²

With the correcting shape factors for drag flow, F_d , and pressure flow, F_p , defined as

$$F_D = 1 - (0.5356 \times n^{-0.4}) \frac{h}{lv}$$

$$F_P = 1 - (0.6216 \times n^{-0.4}) \frac{h}{lv}$$

Equation 31: Drag and Pressure Flow Correcting Shape Factors¹²

With lv being the channel width. Pressure drop across the die was also calculated. Bubble expansion occurs due to the pressure gradient between vapor pressure and outside pressure components, which include elastic (P_e), yield (P_y), and tensile stress ($\frac{2\sigma}{R}$) as well as atmospheric pressure (P_a)¹². Moisture within the melt is converted into steam during cooking, and a bubble matrix forms. In this model, all bubbles were assumed to be uniform in size and shape. When pressure acts in the outward direction, expansion occurs, and shrinkage occurs when pressure acts inward. The rate of expansion is calculated as $P_w - P_a - P_e - P_y - \frac{2\sigma}{R}$ and the rate of shrinkage found by $P_a + P_e + \frac{2\sigma}{R} - P_w - P_y$ ¹². Elastic stress and yield stress were determined by the following equations

$$P_e = \left[\frac{5}{2} - \frac{2R_0}{R} - \frac{1}{2} \left(\frac{R_0}{R} \right)^4 \right] \left(\frac{L^3 - R^3}{L^3 + 2R^3} \right) \quad (\text{elastic stress})$$

$$P_y = 3.464 \tau_0 \left[\frac{1}{3} + \ln \left(\frac{L}{R} \right) \right] \quad (\text{yield stress})$$

Equation 32: Elastic and Yield Stress¹²

The rate of change of the bubble radius via expansion was found by

$$\Delta R = R (\Delta t) \left[\frac{P_w - P_a - P_y - P_e - \frac{2\sigma}{R}}{4 \left(\frac{2}{\sqrt{3}} \right)^{n-1} \frac{1}{n} [\xi + K_c - K_s \left(\frac{R}{T} \right)^{3n}]} \right]^{1/n}$$

Equation 33: Rate of Change of Bubble Radius¹²

And bubble shrinkage by

$$\Delta R = R (\Delta t) \left[\frac{P_a + P_e + \frac{2\sigma}{R} - P_w - P_y}{4 \left(\frac{2}{\sqrt{3}} \right)^{n-1} \frac{1}{n} [\xi + K_c - K_s \left(\frac{R}{T} \right)^{3n}]} \right]^{1/n}$$

Equation 34: Bubble Shrinkage Rate¹²

Diffusion of water takes place during the cooking process. As the moisture content in the extruder converts to steam, it moves into a bubble. As the bubble fills with steam, diffusion occurs in the inward direction within the spherical layers of the bubble¹². This model linked microscopic parameters to macroscopic ones. The expansion ratio is then calculated

$$ER = [1 - f_0]_k \left(\frac{L_k}{L_0} \right)^3 + \sum_{j=1}^k (\Delta f_0)_j \frac{L_j^3}{L_0^3}$$

Equation 35: Expansion Ratio (Macroscopic and Microscopic Parameters)¹²

Here, f_0 is the open cell fraction, and L is the bubble's radius. The sectional expansion ratio was defined as the ratio of the extrudate cross-sectional area to the die opening cross-sectional area¹². The model showed that specific mechanical energy and die temperature decreased when the moisture content is increased. Conversely specific mechanical energy increased with screw speed. The expansion ratio decreased with increased moisture content and reduced as the die temperature is reduced. It also increased with an increase in screw speed since an increase in screw speed let to an increase in die temperature. The model also determined that the bubble radius decreased as moisture is added and increased as the screw speed increased. Cell wall thickness decreased as moisture content is reduced and screw speed is lowered¹². The authors noted that a way to improve this model is to better determine the viscosity of the melt.

Krsitiawan et al. built a twin screw extrusion model using numerical software to predict melt temperature and specific mechanical energy. They assumed that flow is either 1D or 2D and occurred locally, that melting began instantaneously before the screw element, and that the melt behaved as a Newtonian fluid. They stressed that a major challenge in predicting extrusion outcomes is the uncertainty of determining viscous behaviors of melts within the extruder¹³. They expressed the volumetric flow rate through the screw channel as

$$Q_v = A\Omega + B \frac{1}{\eta} \frac{\Delta P}{\Delta \theta}$$

Equation 36: Volumetric Flow Rate Through Screw Channel¹³

with A and B being coefficients related to screw geometry and Ω as the speed of the screw rotation. The first term accounts for drag flow, while the second term accounts for pressure flow¹³. An energy balance can determine the temperature changes in the process, with E_v being viscous dissipation, E_{cd} being conduction heat transfer to the barrel, and W being the power dissipation in the volume, V, of the screw element.

$$C_p \Delta T + E_{cd} = E_v = \frac{W}{\rho_m Q_v}$$

$$W = \int_V \eta \dot{\gamma}^2 dV$$

Equation 37: Energy Balance and Power Dissipation Through Screw Channel¹³

The authors started their computation at the exit of the die and moved backward to determine pressure and temperature of each section of the extrusion process. They then compared the temperature at the melting point to their model to check for accuracy. Using the power law, they determined starch melt viscosity based on shear rate, consistency, K, and the flow index, n¹³.

$$K = K_o \exp\left(\frac{E}{R} \left(\frac{1}{T_a} - \frac{1}{T_o}\right) - \alpha (MC - MC_o) - \beta (SME - SME_o)\right)$$

$$n = n_o + \alpha_1 T + \alpha_2 MC + \alpha_3 SME + \alpha_4 T MC + \alpha_5 T SME + \alpha_6 MC SME$$

Equation 38: Melt Consistency and Flow Index¹³

Here β is the thermomechanical history coefficient, and n_o and α are constants that account for the flow index dependency. They determined melt temperatures with 10% accuracy and SME

values with 35-65% accuracy. The large delta in accuracy for SME is largely accounted for by neglecting the raw material's solid transport and friction energy. They modeled melt viscosity at the die exit with predicted temperature and SME values. They concluded that higher temperatures increased expansion for legume-based melts, while the opposite was true for starch-based melts¹³.

Ma et al. investigated extrusion cooking using wheat samples in a twin screw extruder and modeled it via a bulk density model and a melt viscosity model. They noted that rheological properties are essential to understanding the extrusion process. They attempted to create a model that works across different types of extruders, assuming that melt viscosity is not dependent on extruder characteristics. They also noted that shear viscosity differences of melts are dependent on specific mechanical energy variations within the same process¹⁴. To determine bulk density, they used a model equation

$$\rho_b = K_1 \left(\frac{T_{die}}{T_o}\right)^\alpha (X_w)^\beta N_s^\gamma \exp\left(\frac{\Delta E}{R T_{die}} + cX_w\right)$$

Equation 39: Bulk Density¹⁴

Where K, c, α , β , and γ were determined using a regression-based analysis and an objective function. This equation is independent of extruder geometry or melt properties. It can be used across different extruders and different melt recipes¹⁴. They then used an RSM model to compare experimental results to their model. The study suggested that specific mechanical energy is proportional to the average apparent viscosity of the melt, average residence time, and the square of the average shear rate. Therefore, higher melt viscosities will result in higher specific mechanical energies. The study concluded that higher melt viscosity led to better expansion and lower bulk density¹⁴. Viscosity was determined by

$$\eta = \eta^* \gamma_a^{n-1} \exp\left(\frac{\Delta E}{RT_m} + cM_d\right)$$

Equation 40: Viscosity Model Equation Based on SME¹⁴

Where η is the apparent viscosity, η^* the reference viscosity, γ the average shear rate, n the behavior index, M_d the moisture content, and c is an experimentally determined parameter¹⁴. This can be rearranged to incorporate die temperature. Using these equations for bulk density and apparent viscosity and using RSM, they modeled extrusion behavior.

Cheng and Friis applied Buckingham's pi-dimensional analysis method to model a twin-screw extrusion process. They limited the parameters they included in their model to temperature, moisture content, specific mechanical energy, and residence time. Because they choose eight parameters and have a matrix of five ranks, they needed to establish three dimensionless groups based on Buckingham's theorem¹⁵. Those groups are below

$$\frac{P_d F_T}{\rho_B \tau N_s}, \frac{F_w}{F_T} \text{ and } \frac{T_d}{T_o}$$

Equation 41: Buckingham Pi Dimensional Analysis of Extrusion¹⁵

With F_w being the water flow rate into the extruder, F_t the total flow rate, T_o the feed temperature, P_d the die pressure, ρ_B bulk density. These three groups represented the extrusion pump efficiency, the moisture content in the material, and the temperature change in the process, respectively. $\frac{\tau N_s}{F_t}$ was used to represent specific mechanical energy¹⁵. They then determined an equation for bulk density that can be modeled

$$\rho_b = K (X_w)^\alpha \left(\frac{T_d}{T_o}\right)^\beta \left(\frac{P_d F_T}{\tau N_s}\right)$$

Equation 42: Bulk Density Equation – Buckingham Pi Analysis¹⁵

with K , α and β being dimensionless coefficients determined through a regression function using experimental and fitted bulk density. This provided a model that can be replicated in different extrusion settings, as opposed to RSM, which can only work in the specific setting it is applied. Their accuracy for predicting experimental bulk density values was within 9%¹⁵. A shear term can also be added to add an additional parameter to the model and improve its overall accuracy.

$$\rho_b = K (X_w)^\alpha \left(\frac{T_d}{T_o}\right)^\beta \left(\frac{P_d F_T}{\tau N_s}\right)^\gamma$$

Equation 43: Bulk Density with Shear Term Added¹⁵

Wang et al. studied the expansion phenomena in starches during extrusion using a model solved by finite element methods. In addition to the aforementioned description of bubbling during expansion, viscous effects of the melt as it exits the die resulted in swelling, which increased the diameter of the extrudate. They described three phenomena happening on a micro scale during the bubbling process: nucleation of bubbles as saturated moisture in the melts induced a pressure

drop, expansion of bubbles by pressure forces acting on the bubble shell, and diffusion of water vapor from the melt into the bubble¹⁶. They proposed that the expansion can be determined from the pressure difference, which is given by

$$\Delta P = \frac{4\left(\frac{2}{\sqrt{3}}\right)^{n-1}}{n} \left(\frac{\dot{R}}{R}\right)^n [\xi + K_{bs} - K_{d's} \left(\frac{R}{\dot{R}}\right)^{3n}]$$

Equation 44: Pressure Difference During Bubbling¹⁶

With \dot{R} being the change in radius over a defined timespan

$$\dot{R} = \frac{\Delta R}{\Delta t} = R \left[\frac{\Delta P}{\frac{4\left(\frac{2}{\sqrt{3}}\right)^{n-1}}{n} [\xi + K_{bs} - K_{d's} \left(\frac{R}{\dot{R}}\right)^{3n}]} \right]^{1/n}$$

Equation 45: Radius Change During Bubbling¹⁶

They established the governing equation of diffusion as

$$\frac{\delta X_{w,d'}}{\delta t} = \frac{1}{r^2} \frac{1}{\delta r} (r^2 D_{w,d'} \frac{\delta X_{w,d'}}{\delta r})$$

$$D_{w,d'} \left(\frac{\delta X_{w,d'}}{\delta r} \right) \Big|_{r=R} = \frac{m_{v,c}}{\rho_s} \frac{1}{4\pi R^2} \quad \text{B.C. 1}$$

$$X_{w,d'} \Big|_{r=R'} = X_{w,d's} \quad \text{B.C. 2}$$

Equation 46: Moisture Diffusion Governing Equation with Boundary Conditions¹⁶

The study noted that rupture will occur if the bubble shell stress exceeds tensile failure stress. Equations to determine both shell stress and tensile failure stress were given¹⁶. The number of open bubbles at a point in time during the extrusion process was determined by

$$\Delta f_{o,i,t} = \frac{\Delta Z_i}{\sqrt{2\pi}} \exp\left[-\frac{Z_i^2}{\psi}\right]$$

Equation 47: Number of Open Bubbles During Extrusion¹⁶

Where $Z_i = S_w - \frac{S_f}{2S_f}$. To model transport phenomena, they used the governing equation of momentum for the downstream melt flow represented as

$$\rho \left(\frac{\delta u}{\delta t} + u \frac{\delta u}{\delta z} \right) = -\frac{\delta P_s}{\delta z} + \frac{1}{r} \frac{\delta}{\delta r} \left(r \eta \frac{\delta u}{\delta r} \right)$$

Equation 48: Momentum Governing Equation Incorporating Bubbling¹⁶

With the assumption made of a non-Newtonian fluid and a symmetrical die¹⁶. Boundary conditions were

$$\begin{aligned}\frac{\delta u}{\delta z} \Big|_{r=0} &= 0 \\ u \Big|_{r=0} &= 0 \text{ (die flow)} \\ \sigma'_{r=R} &= 0 \text{ (free-surface flow)}\end{aligned}$$

Equation 49: Boundary Conditions for Momentum Equation¹⁶

The authors also attempted to model the diffusion of water in the extrudate by using the equation

$$\frac{\delta X_{w,e}}{\delta t} = \frac{1}{r} \frac{1}{\delta r} \left(r D_{w,e} \frac{\delta X_{w,e}}{\delta r} \right) + X_{v,e}$$

Equation 50: Moisture Diffusion in the Extrudate¹⁶

They considered the moisture loss in the expansion process in three key areas: evaporation in closed bubbles during expansion, evaporation via the barrel surface to the ambient environment, and diffusion to the surface of the extrudate as a liquid and then release as a vapor to the atmosphere. All three of these components were accounted for in their modeling equation¹⁶. To model heat transfer, they incorporated three components: generation of heat due to evaporation in bubbles, conduction through the extrudate, and release of heat from the surface of the extrudate due to convection¹⁶. Fourier's law with a heat generation term in cylindrical coordinates was used to model this behavior.

$$\rho c_p \frac{\delta T}{\delta t} = \frac{1}{r} \frac{\delta}{\delta r} \left(r k \frac{\delta T}{\delta r} \right) + \dot{q}$$

Equation 51: Heat Transfer Governing Equation (Fourier's Law)¹⁶

Assuming that the die temperature was equal to extrudate temperature as their initial condition and the following boundary conditions

$$\begin{aligned}k \frac{\delta T}{\delta r} \Big|_{r=0} &= 0 \\ k \frac{\delta T}{\delta r} \Big|_{r=R_e} &= h_f (T_{es} - T_a) + q'_{es}\end{aligned}$$

$$q'_{es} = \lambda \frac{m_{w,es}}{A_{es}}$$

Equation 52: Boundary Conditions for Heat Transfer¹⁶

The latent heat of melt solidification was neglected in the model as it was considered very small compared to water vaporization¹⁶. The model was run via computer software with four components: input, bubble growth, bubble growth with extrudate expansion, and transport phenomena in the extrudate. They noted that as extrudate leaves the die, the shear rate rapidly approaches zero as it encounters free surface flow. To improve model accuracy a rheological correlation for low shear rate, die swell and bubble growth must be chosen. Another facet that could lead to deviations between experimental data and model output is the concept of moisture loss. During the melting process, moisture content at the exit of the die could be different from moisture content at the feed as moisture is lost due to evaporation¹⁶. This must be accounted for in any model. Finally, the study identified expansion trends and determined that extrudates expand radially instead of longitudinally during the extrusion process. Their model's velocity profile showed three distinct sections. First, as the melt goes through the die opening, a high shear rate caused by the high viscosity of the melt acted on the melt along with friction from the die wall. This resulted in a parabolic velocity distribution. As the melt exited the die, it entered into a free surface flow regime. This shifted the velocity distribution profile from a parabolic distribution to a uniform one¹⁶.

Kristiawan et al. reviewed various models for the expansion process that involved both a macro and micro-level modeling technique. They asserted that many models are based on an equation for the bubble growth radius of a single bubble

$$R\ddot{R} + \frac{3}{2} \dot{R}^2 = \frac{1}{\rho} (P_G(t) - P_\infty - \frac{2\sigma}{R} - 4\eta \frac{\dot{R}}{R})$$

Equation 53: Bubble Growth for a Single Bubble¹⁷

Where \dot{R} is the time derivative and \ddot{R} is the second derivative of the bubble radius with respect to time. σ is the surface tension, and η the liquid viscosity. This equation shows that surface tension and viscosity limit radial expansion during the initial expansion stages¹⁷. As the bubble grows, the growth rate is then limited by liquid acceleration. The above equation cannot be applied to

modeling multiple bubbles. To model multiple bubbles, the momentum equation for multiple expanding bubbles was represented as

$$\dot{R} = \frac{V+R^3}{4\eta V} [(P_G - P) R - 2\sigma] - \frac{R}{3} \frac{d \ln \rho}{dt}$$

Equation 54: Bubble Growth for Multiple Bubbles¹⁷

This assumed an ideal gas within the bubble, that Henry's law applied at the gas-liquid interface, with no gas loss to the surrounding environment, and it neglected inertial effects, surface viscosity, and elasticity. Here V represents the volume of the cell envelope¹⁷. This model showed that the ratio of the pressure differential between the inside and outside of the bubble to the viscous forces of the melt determined the bubble growth rate. What makes this model more advanced is it accounts for the depletion of dissolved gas and the thinning of bubble walls during the bubbling process. The authors noted that in other bubbling models, one must take into account shrinkage, which occurs after rapid vaporization of the moisture in the bubble. The bubbles shrink after expansion by the vapor cooling, which creates a negative pressure differential between the bubble and the surrounding elements. The most comprehensive models that were reviewed coupled a microscopic model for bubble growth with a macroscopic model for transport phenomena (heat, mass, and momentum transfer). For example, the authors noted that one can create a model on the micro scale to simulate the diffusion of CO₂ and water vapor into a bubble as it grows and couple this with a macro model to predict melt flow, bulk diffusion of CO₂ and water to the atmosphere, and the temperature profile inside the extruder barrel, all of which are governed by transport phenomena equations¹⁷. The authors put together their own model to incorporate rheological properties during expansion. To do this, they used the output variables of foam density and the anisotropy factor, defined by a relationship between longitudinal and radial expansion¹⁷.

Singha et al used the Hybrid Mixture Theory (HMT) to develop a model to understand the extrusion process. The HMT uses a combination of micro, meso, and macro equations to effectively model the expansion process within an extruder. They used a generalized form of Darcy's equation for each gas, solid and water phase to create a mass balance equation to be modeled¹⁸.

$$\frac{D^S (\epsilon^x \rho^x)}{Dt} + \nabla E (\epsilon^x \rho^x V_E^{x,S}) - \epsilon^x \rho^x \frac{\dot{\epsilon}^S}{\epsilon^S} = \sum_{\beta=w,g} \hat{e}^\alpha$$

Equation 55: Generalized Form of Darcy's Equation¹⁸

Here $\frac{D^S}{Dt}$ and $\dot{\epsilon}$ represent the material time derivative with respect to the solid phase, v is the Eulerian velocity, and ∇E is the spatial gradient¹⁸. Each phase carried with it assumptions that modify the above equation. Similarly, velocity was modeled also using a form of the Darcy equation for each phase

$$V_E^{w,S} = (\epsilon^w \frac{K^w}{\mu^w} \nabla \epsilon \rho^w + \epsilon^w D^w \nabla E \epsilon^w + \epsilon^w \frac{K^w}{\mu^w} N^w \nabla E \dot{\epsilon}^w)$$

Equation 56: Darcy Equation for Velocity¹⁸

An energy balance equation driven by convection, conduction, and phase change was represented by

$$\sum_{\alpha=s,w,g} \epsilon^x \rho^x C_p^x (\frac{\delta T}{\delta t} + V_E^x \nabla E T) = \nabla E \sum_{\alpha=s,w,g} (\epsilon^x k^x) \nabla E T - \lambda^w \hat{e}^g$$

Equation 57: Energy Balance of Extrusion with Convection, Conduction, and Phase Change¹⁸

Here the first term on the left side of the equation is the energy storage term, and the second accounts for convection. The first term on the right-hand side represents conduction, while the second represents the energy sink due to evaporation and condensation¹⁸. Their momentum balance equation is shown below

$$\sum_{\alpha=s,w,g} \rho^x \frac{\delta^2 u}{\delta t^2} - \nabla_L \sigma = F_b$$

Equation 58: Momentum Balance with Phase Change¹⁸

where σ is the stress tensor and F_b is the body force. u represents the displacement field, which is a function of internal stress. They determined the heat transfer coefficient by solving for a Nusselt number relation for axial convection through a cylinder and modeled moisture content and expansion ratio via computer simulation¹⁸.

$$\text{Nu} = \left[0.6 \frac{L}{D}^{0.5} + 0.387 \left(\frac{\text{Ra}}{\left[1 + \left(\frac{0.492}{\text{Pr}} \right)^{9/16} \right]^{16/9}} \right)^{1/6} \right]^2$$

Equation 59: Nusselt Number for Axial Convection Through a Cylinder¹⁸

Singha et al. created a design model to depict the changes to moisture content, extrusion temperature, screw speed, mass flow rate, and SME during the extrusion process when adding distilled dried grains (corn) as a protein supplement. They introduced an equation to solve for SME with

$$\text{SME} = \frac{\Omega \omega}{\text{MFR} \left[\frac{3600}{1000} \right]}$$

Equation 60: Specific Mechanical Energy (SME)¹⁸

which is based on the net torque, Ω , of the screw drive, the angular velocity of the screw, ω , and the mass flow rate of the extrudate. To determine apparent viscosity, they tailored a viscosity equation with screw geometry¹⁸.

Ditudompo et al introduced an equation for shear stress that incorporates screw geometry using the equation

$$\tau_s = \frac{\Omega}{2\pi (r_{\text{coor}})^2 L_s} = C_{ss} \Omega$$

Equation 61: Shear Stress Incorporating Screw Geometry¹⁹

Where r_{coor} is based on the effective radius of the screw and C_{ss} is an empirical correction factor for shear stress¹⁹. Apparent viscosity is then determined after shear stress is solved for by the following ratio

$$\eta_{\text{app}} = \frac{\tau_s}{\gamma_s} = \frac{C_{ss} \Omega}{C_{sr} \omega}$$

Equation 62: Apparent Viscosity¹⁹

Wilczynski et al. discussed a global modeling approach to extrusion, which broke the extrusion process into multiple components with separate models. These components consisted of solid transport, polymer melting, and melt flow, which can be broken down into multiple components

to be modeled. They proposed this global modeling technique can be solved with a coupled discrete element method and computational fluid dynamics modeling system²⁰.

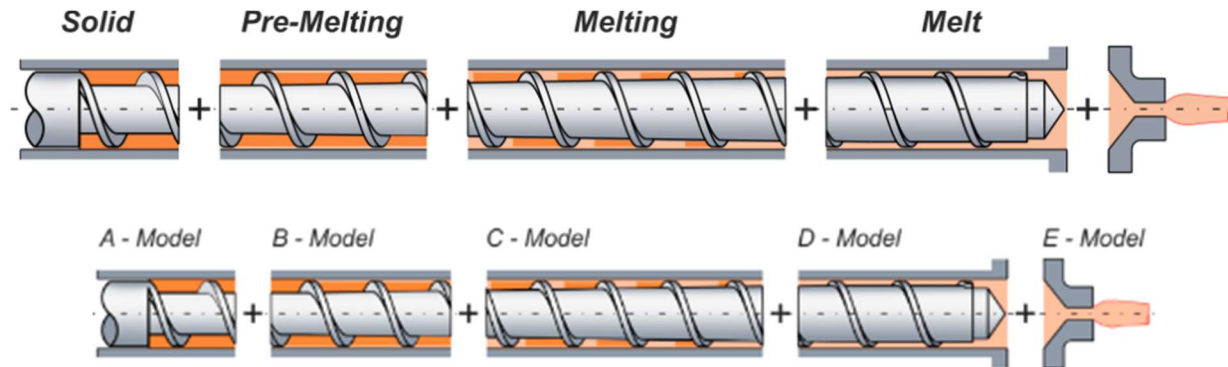


Figure 2: Partitioned Modeling Sections of Extruder²⁰

Pricci et al. delved into the discrete element method (DEM) and computational fluid dynamics (CFD). They stated the limitations of DEM are the need to know the coefficient of restitution, friction coefficients, and determination of an appropriate contact model as factors that need to be determined in order to properly set up a model²¹. DEM allows unlinking particles from a mesh system, which other common computational techniques cannot. They pointed to CFD as a way to incorporate complex geometries into a model as well as to incorporate slippage boundary conditions, as most extrusion models assume no-slip boundary conditions, which may not be a reality depending on the conditions of the extruder system and material being used. As shear stress increased during the extrusion process, slip conditions begin to appear²¹.

Hyvarinen et al. conducted a general review of the current polymer extrusion models. They stated that a flow process in an extruder can be broken down into four sections: the feed into the extruder, the transport section, the flow through the die, and finally, the exiting process out of the die. The extrusion/transport section can further be broken down into the feed, transition, and metering zones²². Each zone is unique in that modeling approaches must change based on geometries, parameters, and phenomena occurring in each zone.

Wilczynski et al. modeled extrusion of wood plastic composites in a single screw extruder using a global modeling approach. Since this composite exhibits slipping effects at the extruder's walls, they considered slip boundary conditions. To model this, they expressed the following equation

$$f_s = F_{Slip} (V_{Wall} - V_s) |V_s - V_{Wall}|^{e_{slip}-1}$$

Equation 63: Shear Stress With Slip Conditions at Walls²³

Where f_s is shear stress, V_s is the tangential velocity of the melt, V_{wall} is the tangential velocity of the wall, and F_{slip} and e_{slip} are parameters of the material. They determined that slippage at the screw and die can impact flow rate and pressure, with flow rate increasing while slippage increased and pressure decreasing²³.

Lewandowski et al. investigated twin screw extrusion and the process of modeling this system. The authors noted that flow is three-dimensional in a twin screw system and unsteady since the screws rotate in either a corotating or counterrotating fashion. To model this effectively, they used computational software that builds a finite element mesh for the barrel but also one mesh for each screw. As a result, they showed different relationships between shear and pressure on the velocity distributions based on whether the system is single, corotating, or counterrotating screws²⁴.

McGuire et al. looked into the effects of particle size of food powders on flow properties within an extruder. They determined that as particle sizes got bigger, the energy needed for flow decreased primarily due to a decrease in surface area, which reduced friction within the extruder barrel. However, the shape of the particle can also affect flow properties, as more rigid shapes with edges can increase friction²⁵.

To deal with the problem of time-varying boundary conditions, which could be present in extrusion, Carr and March developed a semi-analytical process using the Laplace Transform coupled with the separation of variables technique to address a multi-layered diffusion problem with time-varying boundary conditions. To solve this, they broke the system into interfaces and external time-dependent boundary conditions with internal boundary conditions at interfacial layers²⁶. As a result, they defined interface functions and solved them as single-layer problems.

Marschik et al. focused on melt conveying in their modeling of the extrusion process for polymers. The authors set up the geometry of the screw in their model by using a flat plate approach, where a single screw extruder is modeled as if the screw channel was connected at its ends to a flat plate⁵¹. This allowed them to use Cartesian coordinates with an x, y, and z direction but introduced an error that grows with the channel depth since the flat plate model does not account for screw curvature. They referenced that viscous forces usually dominate in extrusion flow over inertial forces, and the resulting Reynolds number is very small. When setting up their conservation equations, they determined that most previous studies neglected viscoelastic effects

primarily due to the computer power needed to incorporate these effects into a model⁵¹.

Assuming a fully developed flow, they modeled the shear rate of the melt below

$$\dot{\gamma} = [2 \left(\frac{\delta v_x}{\delta x}\right)^2 + \left(\frac{\delta v_x}{\delta y} + \frac{\delta v_y}{\delta x}\right)^2 + 2 \left(\frac{\delta v_y}{\delta y}\right)^2 + \left(\frac{\delta v_z}{\delta x}\right)^2 + \left(\frac{\delta v_z}{\delta y}\right)^2]^{0.5}$$

Equation 64: Shear Rate of Melt Flow with Viscoelastic Effects⁵¹

They noted that in large extruders, the Peclet number ($>10^4$) is high, and convective heat transport becomes the primary means of heat transfer. In these cases, heat transfer can be modeled as

$$\rho c_p v_z \frac{\delta T}{\delta z} = \lambda \frac{\delta^2 T}{\delta y^2} + \tau_{yx} \frac{\delta v_x}{\delta y} + \tau_{yz} \frac{\delta v_z}{\delta y}$$

Equation 65: Heat Transfer in Large Extruders with High Peclet Number⁵¹

They graphically mapped the velocity distribution in the melt conveying section using a drag flow and pressure flow term⁵¹.

Eitzlmyer et al. developed a mathematical model for pharmaceutical melts to measure pressure in a filled extruder. Their model aimed to produce results of pressure gradients by approximating parameters that could not be fitted to experimental data. They modeled the pressure gradient within the extruder as

$$\left(\frac{\Delta P^*}{\Delta x^*}\right) = \frac{\Delta P}{\eta n \Delta x}$$

Equation 66: Pressure Gradient in Twin Screw Extruder⁵²

with η being the dynamic viscosity of the melt and n being the screw speed. They assumed a creeping flow regime (low Re number), a Newtonian fluid, and a flow geometry that is geometrically symmetrical. To model non-Newtonian fluids with shear thinning, they modified the above equation. They defined parameters A_1 and A_2 to account for screw geometry and the Carreau model to account for shear thinning, replacing the dynamic viscosity term.

$$\frac{\Delta P_{c*}}{\Delta + x^*} = \frac{\Delta P}{\eta_o n \Delta x} = \frac{A_2 \left(1 - \frac{V^*}{A_1}\right)}{\left[1 + \frac{Y}{Y_{crit}}\right]^m}$$

Equation 67: Modified Pressure Equation Incorporating Carreau Model⁵²

They then estimated the parameter A using a 2D model of flow between two parallel plates, indicating the approximation had very little effect on the modeling of the pressure gradient. They included equations for shear wall stress and the effects of temperature on viscosity. They found that the melt temperature is much higher than the screw temperature due to viscous dissipation within the melt. The pressure gradient increased with screw speed but decreased with throughput⁵².

Methodology

1. Overview Widely Used Cooking Forms

There are numerous widely used cooking techniques within the food industry. Boiling water cooking consists of a batch vessel that holds a product to be cooked in addition to water. Heat is applied and as the water begins to reach its boiling point, heat transfer occurs through the water and steam generated in the process. This heat is transferred to the food product. Pressure is typically close to atmospheric, and of the mainstream cooking processes, boiling produces very low shear stresses due to the low viscosity of water. There is also no mechanical energy generated due to the low shear. Heat convection and conduction are the primary drivers of cooking³⁴. This results in a slow but gentle process which results in minimal impact on the cooking products' cell structure.

Steam cooking is similar to boiling water cooking, but steam is the primary driver of the cooking process and not water heating. Here, steam is fed to a jacket or barrel filled with product, and heat conduction and convection set in to begin the cooking process. This creates more pressure than the boiling water technique and more shear. As a result, the cooking time is faster, but the product has more structural changes, and more moisture is added³⁴. Steam cooking is done in a batch reactor and requires residence times of over an hour. The long cooking times are a disadvantage of this process³⁴.

There are also newer forms of cooking that have started to gain traction in the food industry in recent years. Infrared heating uses infrared radiation (located between the UV and microwave wavelengths), which converts to heat upon impact with food surfaces. Wavelengths are modulated to control the heating mechanism. The wavelengths hit directly on the surface, negating the need for a heat transfer medium. Upon impact, molecules see an increase in movement, increasing internal energy and hence temperature within the product. The benefits of IR cooking are it provides uniform heating across surfaces, has a very high heat transfer rate, uses minimal water compared to other popular cooking forms, and is relatively quick³⁵. The downside is that IR wavelengths do not penetrate the product body, preventing a thorough cooking process from taking hold³⁵.

Microwave heating is a common cooking technique that has been around for decades. It is very cheap and relatively quick. In microwave applications, an electromagnetic field is created that transfers electricity to the food product at a molecular level. This creates rotation and then collision amongst polar particles. Ionic conductivity accelerates water molecules in the food product and induces collisions, creating heat³⁵. Microwave heating technology is fairly developed. The process is quick, relatively cheap, and preserves many important nutritional and sensory characteristics within food products³⁵. Because the heating process is so quick, products that are not uniformly shaped or do not have uniform water distribution within their bodies can be susceptible to burning³⁵.

Ohmic heating is an emerging technology in the food industry. The premise of ohmic heating is based on inducing an electric voltage into a food product which creates a current. This current flows through the product and creates electrical resistance. Based on this resistance, heat is generated³⁵. While it is an old technology first experimented on in the 19th century, it is currently re-emerging in the food industry. The benefits include short cooking durations due to the speed of heat transfer, a uniform cooking process, and substantial energy efficiency compared to other cooking applications. Ohmic cooking can reduce energy consumption by an estimated 70% compared to commercially available cooking applications like extrusion. However, the current can cause thermal shock, damaging cell walls and potentially disturbing food characteristics³⁵.

2. Polymer Extrusion History

The study of polymers in the extrusion process is much more advanced than plant-based meats and can lend valuable insight into extrusion heat and mass transport phenomena that can be incorporated into mathematical models. Polymers are much more predictable than plant-based meats due to their homogeneous structures in addition to well-developed characterizations of their physical and rheological properties. When it comes to plant-based extrusion products, the complex interactions of biomolecules within the extruder under heat and stress are not as clearly understood¹².

The extruder setup for polymers is akin to what is used in plant-based meats. Heat is applied as the polymers are fed into the barrel, and they begin to melt and mix via the screw. The mixing mechanism is how complex and advanced polymers or polymer composites are formed²⁰. In the solid conveying section, polymer solid particles are compacted to form a bed that flows through

the barrel due to forces applied by the screws and heat from the barrel. The polymer then enters the melting section, where it begins to melt, forming a melt layer between the barrel and the rest of the solid body of the melt. Heat conduction continues to melt this solid portion of the melt along with viscous dissipation²⁰. Once fully melted, it enters the melt conveying section and then into the die. Chemical reactions play a significant role in polymer extrusion, as many polymers are mixed in an extrusion process to form new polymers. Internal (shearing and mixing) and external (applied heat to the barrel) heat provide energy to kick start chemical reactions during extrusion³⁸.

One key difference in the research fields between polymer extrusion and food extrusion is the extensive knowledge gained on the rheological properties of polymers during extrusion. Rheology greatly impacts polymer molecular mass distribution, chain branching, and cross-linking. As shear stress increases action on the melt, the melt's volume will increase along with its viscosity and eventually reach a maximum³⁶. Most food-based models on extrusion assume instantaneous melting. With polymers, it has been shown that melting occurs from the outside in. As the melt moves along the barrel, the solid mass decreases, and the melt mass increases, which is known as drag-induced melt removal. It is also broadly accepted that there is a transition region between solid and melt³⁷. Extensive models detail heat and mass transfer and viscosity in each of the three polymer regions³⁷. Common mathematical techniques used to solve polymer extrusion models include the Finite Elements Method, Finite Volumes Method, and Discrete Elements Method³⁷. In addition, many polymer models break their modeling techniques down into a solid region, a transition zone, and a melting region with accompanying heat and mass transfer phenomena equations for each. Recent investigative research has focused on the nanoscale effects of stresses during the extrusion process and its effect on rheology, where studies of extrusions of foods have not been fully reached. Reactive extrusion studies have also gained traction in recent years. Polymer extrusion also uses a triple screw setup in some cases, which is not common in food extrusion. Triple screw extrusion provides increased residence time for polymers in the extrusion barrel. It also increases shear stress and has been shown to have a high plasticization efficiency. They are ideal for polymers with high viscosities³⁸.

A brief overview of polymer extrusion mathematical modeling approaches follows. Toukhtarian et al. use a Lagrangian-Eulerian finite element method to model Newtonian fluids with a changing die gap parameter. Here, the die opening width is varied during the extrusion process to

control the polymer shape. ALE method combines both Eulerian and Lagrangian methods to develop a mesh that flows with the melt along the extruder. The governing equations are spatially discretized, and a predictor multi-corrector method is used to solve the equations. Because a fine mesh is needed, the simulation takes days to weeks to complete. The authors propose a free surface interpolation technique to cut down on the simulation time by adding more nodes to the mesh⁴⁰. Wilczynski et al. incorporate slip conditions in their models of composite wood polymers. A power law model is used to determine the slip-like behavior of melts within the extruder and is incorporated into equations to determine viscosity and shear stress to more accurately determine predicted viscosity and flow⁴¹. Amangeldi et al. developed a velocity and temperature distribution model for polypropylene melt to determine optimal steady-state flow conditions. A Crank-Nicholson method using the central difference method with Dirichlet boundary conditions is used to solve the governing heat transfer equation. It is determined that high starting temperature and larger barrel radius are the primary drivers to help the melt reach steady state faster⁴². Zairi et al. investigate equal channel angular extrusion and how geometry affects the extrusion modeling process. They develop a plastic constitutive response equation and a stress factor between material ligaments to assist in modeling deformation and expansion, with the end state modeling a polymer's deformation during extrusion.⁴³ Hosseini et al. use a least squares method to develop a stress-strain equation. They proceed with the finite element method using static codes to solve their equations. They couple these results with an analysis of variance technique to optimize experimental parameters⁴⁴. Abeykoon et al. developed a model to show the nonlinearity of the temperature profile in the extruder die, which is difficult to measure manually. They couple a polynomial function with a Linear-In-The-Parameters estimation technique to develop a temperature profile at various points in the die section. They are able to determine that melt temperature profiles are affected first by screw speed, then by barrel temperatures⁴⁵. Mu et al. develop a 3D model for viscous flow using computational fluid dynamics. Utilizing a Cauchy stress tensor, the authors define governing equations for momentum and energy and employ the Carreau model for viscosity. Using the finite element method to solve with a function to suppress data oscillations to facilitate convergence, they can develop flow profiles for the polymer melts with a metal insert⁴⁶. Mu et al. simulate starve-fed single-screw extrusion of polymers by developing a mathematical model. They take an iterative approach using lumped parameter modeling. They also propose two

different models, one for the partially filled area of the process and one for the completely filled (with melt) area, as the phenomena are different between regions. Since starve-fed extrusion has a known input, a forward/backward calculation technique is performed until both the forward and backward calculations are equal. This allows them to show categorically that starve-fed extrusion results in faster fusion than flood-fed extrusion ⁴⁷. Kadyirov et al. craft a model for the metering zone in a single screw extruder to analyze the effects of screw geometry and pressure drop on flow. Using a 3D governing equation of momentum that incorporates pressure, viscosity, and density, they incorporate the Cross model for viscosity, which considers the melt's rheological behavior during extrusion. They determine that the axial velocity vector is the least sensitive compared to the radial and tangential vectors. Software is then used to develop a mesh that converges, and various screw geometries are used as input parameters. This develops a flow profile that shows a direct correlation of rotational velocity on pressure and velocity profile⁴⁸. Roland and Miethlinger use modeling tools to profile viscous dissipation in the melt conveying zone. Velocity is divided into a cross-channel and a down-channel component. A deformation tensor rate is defined, affecting the shear stress and hence the governing equation. Viscous dissipation is then solved via the energy equation. The theory of similarity is applied to nondimensionalize the governing equations, and the finite difference method is then used to solve and compare to an analytical solution.⁴⁹ This method allows the authors to develop a profile of viscous dissipation in the melt. Hammer et al. construct a digital twin to model various phenomena in polymer melt extrusion. They nondimensionalize governing equations and determine that four dimensionless input quantities adequately describe the extrusion process: the two viscosities of two different fluids, the position of the interface, and the ratio of pressure gradients. Solving these equations via computer software, they are able to use the results as inputs to their digital twin⁵⁰.

3. Extruder Basics

Extrusion cooking is one of the main avenues for producing plant-based meat alternatives. It is popular primarily since very little nutritional value of food is lost during the process³⁰. Extrusion lends additional benefits compared to other cooking forms in that it can produce different shapes, textures, and colors by altering operating conditions, is a fairly low-cost process, takes up less space than alternative cooking mechanisms, can be easily automated, and creates very little

waste⁸. The basic extrusion mechanism consists of a screw, barrel, and die. A food product is placed into an extruder while a screw or twin-screw mechanism creates movement in the product. This is done by a feed hopper that feeds the product into the barrel³¹. The product, called a melt inside an extruder, is subjected to mixing, shearing, cooking, and compression, and finally is forced through a die at the exit of the extruder, where it expands³⁰. A die is a small opening that the melt is forced through. A restrictor plate is placed at the end of the barrel, which helps to force the melt through the die³¹.

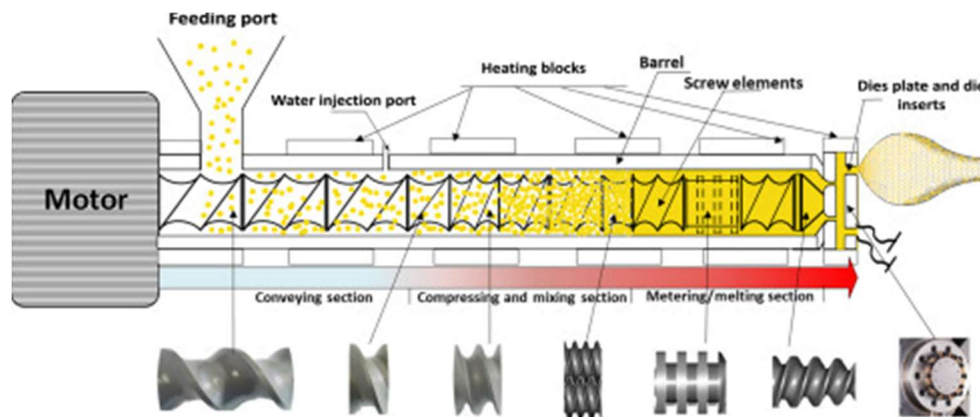


Figure 3: Common Extruder Schematics³⁹

There is a combination of three different flow regimes inside an extruder. These are pressure flow, drag flow, and leakage flow²¹. In drag flow, there is friction created between the melt and the barrel surface as the melt is pushed through the barrel. Leakage flow occurs due to the gap between the screw and the barrel and is larger as the gap grows. During the extrusion process, the Maillard reaction typically occurs between the melt's reducing sugars and the free amino groups of proteins in the melt. This is what gives plant-based products their brownish color²⁸. The extrusion process aims to make the plant protein melt as close to animal meat in taste, texture, color, and feel as possible. Proteins are hydrated and mixed via the feeder and screw configuration as they enter the extrusion process. They begin to lose their organized shape and become a viscous melt from the effects of heat and shear stress brought on by the screws³². As the protein complexes break down, denaturation and gelatinization occur within the melting zone. As the melt exits the barrel, it traverses through a die as it exits the extruder. The temperature of the melt decreases as it moves through the die channel, and the viscosity is increased²⁸.

To summarize the physics of the extrusion process, water is added to the melt and mixed. Heat is then applied to the melt, and viscous dissipation sets in within the conveying section. Expansion occurs in the transition and cooling zones as water is turned to steam, and bubble growth sets in. Expansion stops once a critical viscosity level is reached as the temperature falls after the die exit¹⁷.

Expansion is a critical process within the extrusion system. The melt is first wetted as it enters the extruder. Next, heat, shear, and mixing forces are applied as the melt moves through the barrel of the extruder. Once it reaches the die, additional shear forces are applied through the die exit, and the melt is finally released outside the extruder system. As it exits, water contained in the melt becomes superheated due to pressure forces, and a pressure differential occurs between the die and the outside environment, which brings on evaporation. This causes expansion due to bubble growth and viscoelastic effects. The melt then collapses due to elastic recovery, and pressure and temperature drop upon exit as evaporative cooling sets in. Finally, a porous plastic-like form emerges as the final product. The porous solid matrix is caused by the interactions between the expanding vapors and moving liquids within the melt with the solid walls of the melt matrix¹⁹. This expansion process is what gives the extrudate its qualities and characteristics.

A. Screw Section

Extrusion systems can consist of one or two screws. The screw is affixed to a barrel, usually cylindrical in shape, with a feeding system that pushes the food product into the barrel³⁰. Two common types of screw formations are single and twin (double) screws. Single-screw extruders are cheaper and easier to operate, while twin-screw extruders give greater control of the process's temperature, pressure, and speed. A wider range of food products can be used with a twin screw setup, including very wet and very dry products, powders, and highly viscous materials³⁰. In a single screw extruder, a screw rotates inside a smooth, fixed barrel. An electric motor with a variable speed drive and reduction gear supplies the mechanical energy to the system³¹. In a twin screw extruder, two screws rotate side by side, and the melt is pushed around the screws in figure-eight, generating significant shear force³². Within the screw itself there is a forward/reverse conveying system that can push the product forward or backward in the barrel. The kneading element, both forward and reverse, of the screw supplies the shear force acting

upon the product. Finally, the pure kneading element helps to restrict flow as the product moves toward the die³².

B. Barrel Section

In some variations of extruder systems, the barrel can have heat bands applied around it to supply the cooking process with added heat³². Within the barrel, thermodynamics plays a role during the cooking process. There are both noncovalent interactions and covalent cross-linking in plant proteins as well as the increased formation of disulfide bonds during extrusion. This will ultimately decrease the solubility of the proteins³⁰. As protein is denatured with increasing heat applied, the surface properties of a melt change and become more hydrophobic. This promotes aggregation, and the plant proteins form a 3D structure that increases their ability to retain water, a key factor in mimicking meat texture³⁰. As screw speed is increased, the degree of fill within the screw lowers, and the amount of time the melt is subjected to thermal treatment within the barrel is reduced³².

C. Die Section

The die section consists of three parts: a tapered transition zone, a non-cooled zone, and a cooling zone³³. As the melt leaves the die, a substantial pressure differential is introduced, which turns water into steam, thus expanding the melt³⁰. The die is meant to subdue the expansion of the melt upon exit. The die section of an extruder consists of the die and an associated cooling zone³². The parameters of the die zone can significantly impact the final shape and texture of the extrudate. Die geometry also plays an essential factor. The cooling die can take on various shapes to help form the final extrudate product. It should also be at a minimum as long as the screw within an extruder ensures that rearranged protein structures are able to be formed during the exiting phase. A shorter die-cooling zone length is associated with more chicken-like meat substitutes, while a longer and thinner die-cooling zone is associated with pork-like meat substitutes³². Pressure profiles can also change the shape of the melt in the die section. It has been observed that if the pressure drop across the die is less than the pressure at the exit of the barrel, the melt length will decrease. Conversely, if the pressure drop is greater across the die

than the barrel exit, the length of the die increases¹². A laminar flow profile is typically observed within the die section, attributed to a Reynolds number less than 1³³.

4. Assumptions

When determining the melt's heat capacity and thermal conductivity, thermal expansion, inertia and gravity were ignored⁷. During expansion, we can assume that pressure and viscosity remain constant¹⁷. To determine viscosity, we assume a plant-based melt is a pseudoplastic power law fluid¹⁶. To determine failure stress, we assume average moisture content remains above 14 percent in plant-based extrusion processes¹⁶. We assume leakage flow is insignificant, and the main drivers of flow are drag and pressure flows¹². We assume the melt behaves as a homogenous non-Newtonian fluid and that we are using a symmetrical die to model momentum. We neglect centrifugal forces associated with the screw and assume that screw curvature is minimal⁹. The fluid is assumed to have laminar flow, and the gravitational and inertial terms of the Navier-Stokes equation are ignored¹¹. To determine the Nusselt number for heat transfer calculations, we assume axial thermal convection that occurs along a cylindrical die¹⁹. We assume a uniform temperature distribution in the extrudate, neglect internal friction between melt particles, melting occurs instantaneously upon reaching the melting point, and convective heat from the barrel is uniformly distributed throughout the melt¹¹. Viscous heat dissipation can be neglected as long as the screws are only partially full. Meaning there is no temperature increase in the conveying section. Complex chemical reactions associated with plant-based meats in the extruder were not incorporated into the models as there is no significant research done into phase transitions, gelatinization, and protein denaturation in terms of mathematical modeling¹². For viscosity, we assume a n_o of .29, K_o value of 8.1×10^5 and α value of 11.4 as these were taken from literature for pea flours¹³. To determine the expansion ratio, we assume that all bubbles created during the expansion process are uniform and spherical and that the longitudinal expansion ratio is equal to 1¹².

When creating our model, we want to take a mechanistic modeling approach. In this approach, we will propose multiple equations to solve to account for transport phenomena taking into consideration extruder geometries and boundary conditions.

5. Model Parameters

When formulating a model, it is important to understand the limitations of the extrusion process when producing plant-based meat alternatives. If the ratio of the thermal diffusivity to the Cahn-Hilliard diffusivity is above 100 or below 1.2, phase separation will not occur and protein delinking will not be observed, rendering the extrusion process ineffective³². Barrel temperature needs to be between 120 and 160 degrees Celsius for complete unfolding³². A temperature below this range will not generate enough thermal energy to kickstart the reorganization of fibrous structures, while a temperature above this range will reduce the viscosity and plant-based product will lose its desired form. Moisture content needs to be between 40 and 80%. Too low of a moisture content leads to an increase in viscosity and corresponding shear forces, deteriorating the final product into a hard mass due to low protein solubility³². Too high of a moisture content will reduce barrel temperature and friction along the barrel, which will prevent protein denaturation. Geometry of the extruder also plays a limiting factor. The length of the die must be at least 60 times longer than the height of the cooling zone. Geometric specifications outside of this range will prevent fibrous matrices from forming³². Lastly, although this model is not focused on plant-based products with additives, it could be applied to that realm. Starch additives, which are a common form of additive to help replicate meat texture, must reach a conversion rate of 37 percent in order to model non-Newtonian flow, which this model assumes.

Limiting Property	Applicable Range
Thermal diffusivity to Cahn-Hilliard diffusivity ratio	1.2 to 100
Barrel Temperature	120 to 160 Celsius
Moisture Content	40 to 80 Percent
Die length to height ratio	At least 60
Starch conversion (additives)	At least 37%

Table 1: Operating Ranges for Computational Model

A. Momentum

As the melt exits the die, the melt cools from the outside in. As a result, there is also a temperature differential between the inside of the die and the external atmosphere. This has a

significant effect on the velocity profile of the melt, as a higher velocity is seen in the interior of the melt³³. A more controlled velocity profile along the extrusion barrel can result in a lower shear rate, ultimately reducing the melt's gelatinization and improving the cooking process⁹.

To model momentum, we use the following equation

$$\rho \left(\frac{\delta u}{\delta t} + u \frac{\delta u}{\delta z} \right) = \frac{\delta P_s}{\delta z} + \frac{1}{r} \left(\frac{\delta}{\delta r} \right) \left(r \eta \frac{\delta u}{\delta r} \right)$$

Equation 68: Governing Equation of Momentum¹⁶

Where ρ is the density, P_s the ambient pressure, u the velocity of the melt, η the viscosity, and r the bubble radius. Using an initial condition of u at $t=0$, $u_0 = 0$ we implement the boundary conditions of $\frac{\delta u}{\delta r} \Big|_{r=0} = 0$ and $u \Big|_{r=R} = 0$ ¹⁶. Both drag flow and pressure flow act on the melt as it traverses through the die. Drag flow is caused by viscous stress and pressure flow by the pressure differential in the die. To determine the pressure gradient, the following continuity equation was used

$$\int_0^R (2\pi r \rho) dr = mt$$

Equation 69: Continuity Equation for Pressure Gradient¹⁶

Velocity can be determined by

$$u = \pi D_b N_s \cos(\phi_b)$$

$$N_s = \frac{L}{l}$$

Equation 70: Velocity Term¹¹

With D_b being the diameter of the barrel, N_s being the flight number (equal to the length of the screw, L , divided by the length of screw flight, l , and ϕ being the axial screw pitch. Velocity will be positive close to the barrel walls as drag flow exists and directs the flow toward the die, while velocity close to the screw surface will be negative in the direction of the pressure flow¹¹. As the melt moves through the barrel, it will decrease in size, and viscosity will also decrease as melting onsets. This will cause a drop in drag flow. To maintain a flow in the direction of the die exit, pressure flow will also decrease to counter the decrease in drag flow¹¹.

B. Shear Rate

As the die diameter to length ratio increases, the shear rate will decrease and vice versa. A higher shear rate will lead to a lower viscosity¹⁷. SME and die temperature will also increase as the shear rate increases, usually associated with increased screw speed. Conversely, die pressure will decrease with an increase in shear rate¹². Within the extruder, the shear rate is high due to the impact of the screws, but it drops significantly and approaches zero after exiting the die due to the onset of free surface flow¹². We can model the shear rate in both the screw and die sections of the conveying section as they will deviate from each other, and the shear in the die will be lower from the following equations

$$\gamma = \left[\left(\frac{\delta u_x}{\delta y} \right)^2 + \left(\frac{\delta u_y}{\delta x} \right)^2 + \left(\frac{\delta u_z}{\delta y} \right)^2 \right]^{0.5}$$

Equation 71: Shear Rate in Screw Section¹¹

$$\gamma = \frac{\delta u_z}{\delta r}$$

Equation 72: Shear Rate in Die Section¹¹

Where u corresponds to the velocity term in the x, y and z directions and r corresponds to die radius.

C. Shear Stress

As the melt exits the die and a temperature gradient develops, there is an increase in shear rates and stress. Tensile stress is more dominant in the interior of the melt as the velocity profile is higher there. Additionally, as the melt moves through the die, it is cooled, and viscosity increases, leading to higher shear stress. Shear stress tends to dominate in the cooling zone of the die, while tensile stress dominates in the transition zone³³. To account for pressure differential, we must incorporate different pressure sources. Pressure differential can be modeled by

$$\Delta P = P_i - (P_s + P_t + P_e + P_y)$$

Equation 73: Pressure Differential¹⁶

Where P_i is the pressure inside a bubble within the melt, P_s is the atmospheric pressure outside of the extruder, P_t represents surface tension, P_e is elastic stress, and P_y is the reduction in pressure caused by yield stress¹⁶. When the shear stress of the melt exceeds the failure stress, bubbles will rupture, and this must be taken into account in our model. To determine failure stress, we can use

$$S_{f,l} = S_m \exp [\alpha_s (T_o - T_i)]$$

Equation 74: Failure Stress¹⁶

Where S_m is a constant of 1,000 kPa, α_s is a temperature shift factor (.013), T_o is ambient temperature, and T_i is the temperature at the shell of the bubbles¹⁶. To determine the shear stress, we use the following equation

$$\tau = \frac{R \Delta P}{2 L_d}$$

Equation 75: Shear Stress⁸

Here R is the radius of the die, and L_d is the length of the die. Apparent viscosity can also be determined from shear stress, which is the ratio of shear stress to shear rate. If the die is of an irregular shape, the hydraulic radius must be used to determine shear stress⁸.

D. Heat Transfer

The temperature within the extrusion process can impact the denaturation, degradation and aggregation of proteins within a melt, all of which contribute to the goal of a meat like texture²⁷. To have a complete unfolding of plant proteins and for crosslinking to occur, a temperature range of 120-160 degrees Celsius has been shown to be ideal³². If the temperature is too low, molecular bonds within the protein will not break down, and the protein structure can't be modified appropriately for meat-like consistency. If it is too high, the viscosity of the melt is significantly reduced, and the extrudate becomes rubber-like in nature³². Heat transfer takes three forms at the macro level: heat generation within the melt due to the evaporation of water in the bubbles, conduction through the melt, and the release of heat from the melt surface by convection, radiation, and evaporation on the surface¹⁶. The temperature will fall as the melt expansion process unfolds when bubbles grow, water diffuses into the bubbles and then evaporates. The latent heat of vaporization associated with this process results in a decrease in temperature¹².

The specific heat capacity of the melt can be determined numerically by the following equation

$$c_p = 1.424X_c + 1.549X_p + 1.675X_f + 0.837X_a + 4.187X_m$$

Equation 76: Specific Heat Capacity of the Melt³³

where X_c is the mass fraction of the carbohydrate in the melt, X_p the mass fraction of protein, X_f the mass fraction of the fat, X_a the mass fraction of the ash, and X_m the mass fraction of the moisture in the melt³³. Thermal conductivity can also be determined similarly, using

$$k = 0.25X_c + 0.155X_p + 0.16X_f + 0.135X_a + 0.58X_m$$

Equation 77: Thermal Conductivity of the Melt³³

To determine a heat transfer coefficient, we can first find the Nusselt number, and if the length and thermal conductivity are known, we can then solve for the heat transfer coefficient.

$$Nu = \frac{h \gamma L}{k_g}$$

$$Nu = \left[0.6 \frac{L^{0.5}}{D} + 0.387 \left(\frac{Ra}{\left[1 + \left(\frac{0.492}{Pr} \right)^{9/16} \right]^{16/9}} \right)^{1/6} \right]^2$$

Equation 78: Nusselt Number Equations¹⁹

To find the Rayleigh and Prandtl numbers, we use

$$Ra = g \beta (T - T_{atm}) L^3 \frac{Pr}{\left(\frac{\mu_g}{\rho_g} \right)^2}$$

Equation 79: Rayleigh Number¹⁹

$$Pr = \frac{c_p^g \mu_g}{K^g}$$

Equation 80: Prandtl Number¹⁹

Here, L is the length of the die, k is the thermal conductivity, D the diameter of the die exit, β a thermal expansion coefficient ($\beta = \frac{1}{T_f}$), T_f our film temperature, ρ_g our density of the melt, μ_g our viscosity, K^g our gas permeability and c_p^g our specific heat capacity of the melt¹⁹. K^g can be

determined below, where s^w is the volume fraction of water divided by the sum of the volume fraction of water and the volume fraction of gas.

$$K^g = 1.01 \times 10^{-3} \exp[-10.86 s^w]$$

Equation 81: Gas Permeability¹⁹

The governing equation of heat transfer is

$$\rho_s c_p \frac{dT_s}{dt} = \frac{1}{r^2} \frac{\delta}{\delta r} (r^2 k_s \frac{\delta T_s}{\delta r})$$

Equation 82: Governing Equation of Heat Transfer in Melt¹¹

Where p is the density of the melt, T_s the temperature, r the radius of the extrudate, c_p the specific heat capacity and k the thermal conductivity. Boundary conditions used include $\frac{\delta T}{\delta r} \Big|_{r=0} = 0$, $T_s \Big|_{r=R_s} = T_m \Big|_{r=R_s} = T_{mo}$, and $k \frac{\delta T}{\delta r} \Big|_{r=R_p} = q_{sur}$.¹¹ T_s is the temperature at the surface of the melt, T_{mo} the initial temperature of the melt, and q_{sur} the heat flux on the surface of the melt¹¹. q_{sur} can be determined by

$$q_{sur} = \frac{Q_b}{N_p A_{p,sur}}$$

$$Q_b = h B_{cn} \Delta z_c (T_{b,sur} - T_{p,sur})$$

$$N_p = \frac{m_z \Delta t}{\rho v_p}$$

Equation 83: Heat Flux at the Surface¹¹

With h being the heat transfer coefficient, z_c being a time step, Q_h the heat term, N_p being the number of particles enclosed, and A being the area¹¹. The velocity of the melt flow can be determined by $\pi D_{bn} N_s \cos(\phi_{bn})$, with D_{bn} being the diameter of the barrel, N_s being the flight number (equal to the length of the screw divided by the length of a screw flight) and ϕ_{bn} the helix angle of the screw channel¹¹.

It should also be noted that particle size plays a role in heat transfer. For small particles (less than 2.5mm radius), convection from the heated barrel surface is the primary mechanism for heat transfer, while for larger particles, convection and conduction within a particle¹¹.

E. Viscosity

It has been shown experimentally that viscosity decreases as temperature increases. It is also a function of the die pressure. As temperature rises, the plant proteins' molecules become more mobile, reducing the viscosity³³.

Viscosity can be modeled using a power law fluid approach

$$\eta = K\dot{\gamma}^{n-1}$$

Equation 84: Power Law Fluid Viscosity Equation¹⁶

Here n corresponds to a flow index between 0 and 1, $\dot{\gamma}$ is the shear rate and K ($\text{Pa}\cdot\text{s}^n$) is the consistency of the melt¹³. The consistency can be determined from moisture content and SME as follows

$$K = K_o \exp\left(\frac{E}{R} \left(\frac{1}{T_a} - \frac{1}{T_o}\right) - \alpha (MC - MC_o) - \beta (SME - SME_o)\right)$$

$$n = n_o + \alpha_1 T + \alpha_2 MC + \alpha_3 SME + \alpha_4 T MC + \alpha_5 T SME + \alpha_6 MC SME$$

Equation 85: Consistency and Flow Index¹³

Here E is the activation energy, R the universal gas constant, T_a is the absolute temperature, K_o the consistency at standard reference conditions, α is the water plasticization coefficient, β is the thermomechanical history coefficient. The standard reference amounts include the moisture content of 10 percent, temperature at 353K and SME at 350 kJ/kg¹³.

F. Specific Mechanical Energy

Specific mechanical energy (SME) in extrusion cooking is defined as a measure of the amount of work (normally from the screws) converted into heat, which is then transferred into the melt³⁰. It positively correlates with heat, so the higher the SME, the more heat is generated. An increase in screw speed will increase SME. Shear rate, temperature, residence time, and viscous dissipation have also been shown to be positively correlated with screw speed and SME³². Modeling SME allows us to consider screw parameters and incorporate them into extrusion effects.

We define SME in our model as

$$SME = \frac{\tau N_s}{F_T}$$

Equation 86: Specific Mechanical Energy¹⁴

Where τ is the torque from the screws, N_s is screw speed and F_T is the mass flow rate of the melt. Viscosity directly influences torque values, which means different melt materials with different viscous properties will have different SME values¹⁴. In addition, SME has been shown in previous studies to be proportional to viscosity, so a higher viscosity in the extrudate will correspond to a higher SME value¹⁴.

Higher screw speed has been shown to produce less “chewiness” in plant-based proteins. It can also lead to greater starch gelatinization, which thins the cell walls of the plant protein and increases the cells’ ability to hold air.⁴ Since SME is a measure of mechanical energy input to a system and is based on the viscosity of the melt, it can be an essential parameter to use when scaling an operation to an industrial capacity¹⁴. Residence time is also an important factor when considering scaling operations. Maintaining the same residence time when scaling procedures is important as it will maintain the melt’s cooking time and temperature shear history in an extrusion process constant¹⁰.

G. Expansion Ratio

Expansion is a critical component of the extrusion process when modeling the process. Expansion of the melt as it moves through the transition and cooling zones is caused by both swelling due to elastic recovery associated with the deformation of the melt in the die and bubble growth. However, bubble growth is the dominant cause of expansion when melts are subjected to high temperatures during food cooking extrusion¹⁷. As the melt passes through the die, pressure begins to decrease as the pressure in the barrel is higher than the die which opens to the atmosphere. If the system pressure falls below the saturating vapor pressure of the melt, water starts to evaporate, and a vapor nucleus forms. This paves the way for bubbles to grow and create a more porous structure in the final extrudate¹⁷. Generally speaking, a higher expansion ratio is more favorable to creating plant-based meats. Parameters affecting the expansion ratio include moisture content, screw speed, and melt temperature. It is inversely proportional to the bulk density of the melt⁴. The higher the pressure differential between the barrel and the die exit (exterior), the higher the expansion ratio of the extrudate product⁴.

Past research has shown that expansion in the die exit will stop once a critical viscosity is reached, typically 10^6 Pa-s¹⁷. In addition, higher moisture contents have been shown to increase

bubble growth in the extrusion process in previous studies. As moisture content is increased, the glass transition temperature is decreased¹⁷. Glass transition temperature controls bubble growth so the lower it is, the easier it is for bubble growth to occur. It has also been shown that expansion cannot occur if the extrudate internal temperature does not exceed 100 degrees Celsius. Additionally, growth will cease at a temperature that is 30 degrees Celsius above the glass transition temperature, which could theoretically be above 100 degrees Celsius¹⁷. As temperature rises, vapor pressure will also increase in the system. This will increase bubble growth¹⁷. Bubbles start to grow slowly upon the melt exiting the die, and growth accelerates as the cell walls start to thin. As the temperature drops after the die exit, vapor pressure within the bubbles decreases and eventually becomes lower than the ambient pressure. Once this threshold is crossed, bubbles shrink until the extrudate takes on its final form¹². Viscosity can have different effects on bubble growth. If the viscosity is too low, the strength of the melt will be too low to keep the bubble shapes, and the bubbles will collapse. If it is too high, it will lead to an increase in pressure in the starch. When the pressure in the starch is higher than the surrounding vapor pressure, ideal bubble growth conditions will not occur¹⁷.

It is important to note that upon exit from the die, the melt will undergo expansion from viscous effects due to the viscoelastic nature of the melt¹⁶. This is in addition to bubble growth caused by the pressure differential of the melt and water vapor.

We incorporate the expansion phenomena into our modeling approach through

$$ER = \frac{D_e^2}{d_{ex}^2}$$

Equation 87: Expansion Ratio¹²

Where D_e is the cross-sectional area of the extrudate and d_{ex} is the cross-sectional area of the die opening¹².

H. Bulk Density

Bulk density can be defined as the ratio of the mass of the extrudate to the extrudate volume. It is an indicator of the porosity of the melt³⁰. There are numerous models in the literature that propose modeling bulk density via a sectional expansion index (SEI), longitudinal expansion index (LEI), and volumetric expansion index (VEI)¹⁵. A higher viscosity in the extrudate has been shown to correlate with lower bulk density in the end product, leading to more expansion

and a stronger porous structure. Higher temperatures and lower moisture content have also been shown to lead to lower bulk density. Changes in SME have shown no significant effect on extrudate bulk density¹⁴. To determine bulk density, we use a regression-based equation

$$\rho_b = K (X_w)^\alpha \left(\frac{T_d}{T_o}\right)^\beta \left(\frac{P_d F_T}{\tau N_s}\right)$$

Equation 88: Bulk Density of the Melt¹⁵

T_d is the temperature of the die, T_o the temperature in the barrel, F_T the mass flowrate of the extrudate product added to the barrel, F_w the mass flowrate of water added to the barrel, N_s screw speed, P_d die pressure and τ the torque of the screw⁸. K , α and β are all experimentally determined coefficients. For the purposes of this model, we will set $K=13,508$, $\alpha=0.7774$ and $\beta=-0.2882$, which were determined by Cheng et al. for experiments with whole wheat flour⁸.

I. Diffusion (Moisture Content)

Moisture content plays a significant role in the formation of quality plant-based meat products. In the context of the extrusion cooking process, moisture content can affect both the flexibility and elasticity of the plant protein. It can also transfer thermal energy, which can lead to reductions in the cooking product's viscosity and shear. As moisture content increases, the plant's fibrous matrix thins out and becomes more meat-like in structure²⁷. As moisture content decreases, a negative effect on tensile strength, hardness, and chewiness has been observed in literature²⁷. As a basis for comparison, meat is approximately 75% water²⁹. A moisture content between 40-80% is needed for high moisture extrusion. If the moisture content is too low, the viscosity of the melt and shear stress acting on the melt is increased, resulting in higher die pressure and a harder end product. If the moisture content is too high, the friction between melt and barrel is reduced along with melt temperature, which inhibits the breakdown of the protein structure³².

As bubbles begin to form through the expansion process, the cell walls of the bubbles thin out. Water vapor diffuses through the bubble wall during this process, moving into the bubble¹⁶.

We propose to model diffusion on a microscale with the following equation

$$\frac{\delta x_{w,d'}}{\delta t} = \frac{1}{r^2} \frac{1}{\delta r} (r^2 D_{w,d'} \frac{\delta x_{w,d'}}{\delta r})$$

Equation 89: Diffusion of Water Vapor into Melt Bubbles¹⁶

We use an initial condition of x_{wd} at $t=0 = x_{w0}$ and boundary conditions of $D_{w,d} \left(\frac{\delta X_{w,d}}{\delta r} \right) \Big|_{r=R} = \frac{m_{v,c}}{\rho_s}$ and X_{wd} at $r=R' = x_{w,d's}$ ¹⁶. Here, R corresponds to the initial average radius of bubbles, R' being the radius including the bubble and shell, x_w being the moisture content, D_w being the moisture diffusivity, ρ_s being the density of the melt and $m_{v,c}$ being the mass flow rate of water vapor into a bubble¹⁶.

$$m_{v,c} = \frac{\Delta \pi R^2}{3 v \Delta t} [3 (\Delta R) - \alpha (\Delta T) + \beta (\Delta x_{w,bs})]$$

Equation 90: Mass Flow Rate¹⁶

Here α is a constant for temperature shift factor, equal to .013 and β a constant for moisture shift factor equal to 73¹⁶. On the macroscale, moisture loss occurs in the extrudate through evaporation from closed bubbles, on the hot surfaces of bubbles and by diffusion to the outer surface of the melt. We use the following equation to model diffusion of water in the melt

$$\frac{\delta X_{w,e}}{\delta r} = \frac{1}{r} \frac{\delta}{\delta r} \left(r D_{w,e} \frac{\delta X_{w,e}}{\delta r} \right) + x_{v,e}$$

Equation 91: Diffusion of Water in the Extrudate¹⁶

With an initial condition of $x_{w,e}$ at $t=0 = x_{w0}$ and boundary conditions of $D_{w,e} \frac{\delta X_{w,e}}{\delta r} \Big|_{r=0}$ and $D_{w,e} \frac{\delta X_{w,e}}{\delta r} \Big|_{r=R_e} = h_m (x_{w,es} - x_{w,a})$ ¹⁶. Here, $x_{w,e}$ is the moisture content in the extrudate, r is the radius of the die, $D_{w,e}$ is the moisture diffusivity, and $x_{v,e}$ is the inner vapor generation rate which takes into account the mass flow rate of water vapor into the bubbles and the mass evaporation rate of water vapor on the walls of open bubbles, It is important to account for moisture loss in our models. The moisture content at the start of the die could be different from the moisture content at the exit¹⁶.

$$x_{v,e} = m_{v,c} N_b (1 - f_{0,n+1}) + m_{v,o} N_b \Delta f_{0,t}$$

$$m_{v,o} = h_e (4 \pi R_0^2) (\alpha_w P_{sat} - P_s)$$

Equation 92: Inner Vapor Generation Rate¹⁶

Here h_e is the evaporation coefficient of water, or 8.4×10^{-7} (kg/(Pa m² s))¹⁶. As the melt expands, there is a decrease in the velocity profile of the melt at the die exit. This is due to a high shear rate and high melt viscosity that creates friction along the die wall. Upon exit, the melt

transitions to free-surface flow with little stress effects. This shifts the velocity profile from parabolic to a uniform distribution. This results in an increase in the diameter of the melt, more commonly known as die swell¹⁶

Results

Calculations were performed in a computational platform with similar modeling parameters as described above using flour and soy bean dough. This computational model used a 1 m long, single screw, cylindrical extruder with an 8 cm inner cylinder diameter. A stress of 20 MPa was supplied at the entrance to the barrel. The die was rectangular in shape. The modeling results for pressure, temperature, and momentum are entailed in this report.

In the figure below, the pressure field is displayed, with a starting pressure of 20 MPa at the entrance to the extruder and a gradual decrease in pressure as the model moves toward the die. Pressure then increases slightly in the die during the expansion process, eventually decreasing again and reaching atmospheric pressure upon die exit.

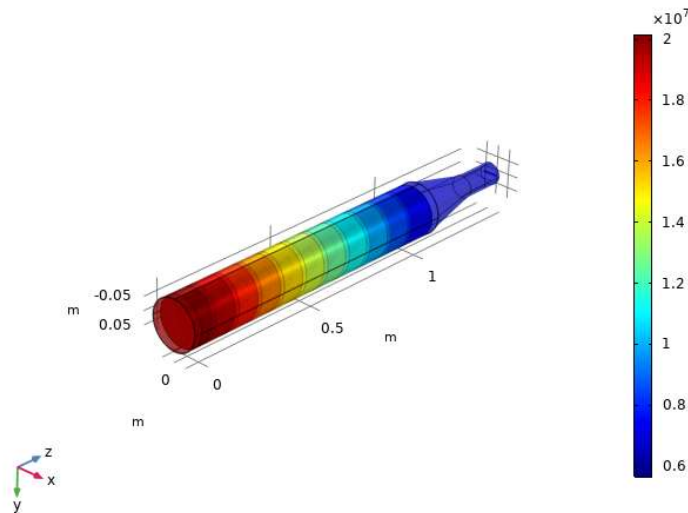


Figure 4 : Pressure Field

The temperature field was modeled and results are shown below. Here, the extruder temperature at the entrance is shown just below 300K. The temperature remains fairly constant throughout the extruder barrel until it reaches the transition zone, where it decreases. In the middle of the die, the temperature increases slightly and immediately decreases again upon die exit.

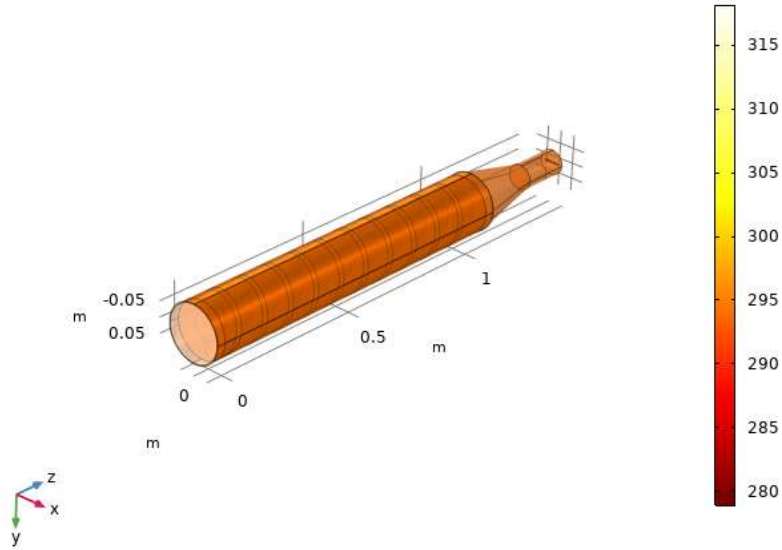


Figure 5: Temperature Field

The yz plane of the temperature field is displayed below. Here, temperature remains fairly constant throughout the barrel, including in the transition zone and die. No major fluctuations are observed.

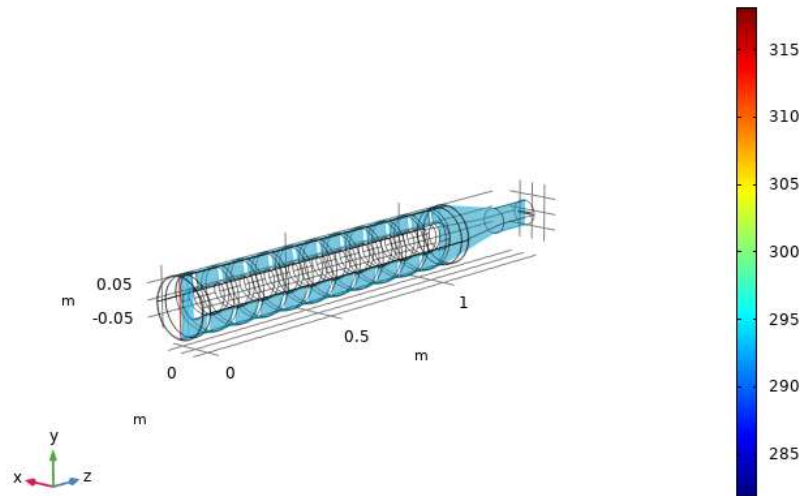


Figure 6: yz Plane of Temperature Field

The xy plane of the velocity field was modeled which is found below. It is observed that velocity on the xy plane remains fairly uniform until the transition zone is approached, where a significant decrease is observed. One can also see decreases in the velocity field as both the screw and barrel walls are approached. Velocity increases slightly in the die.

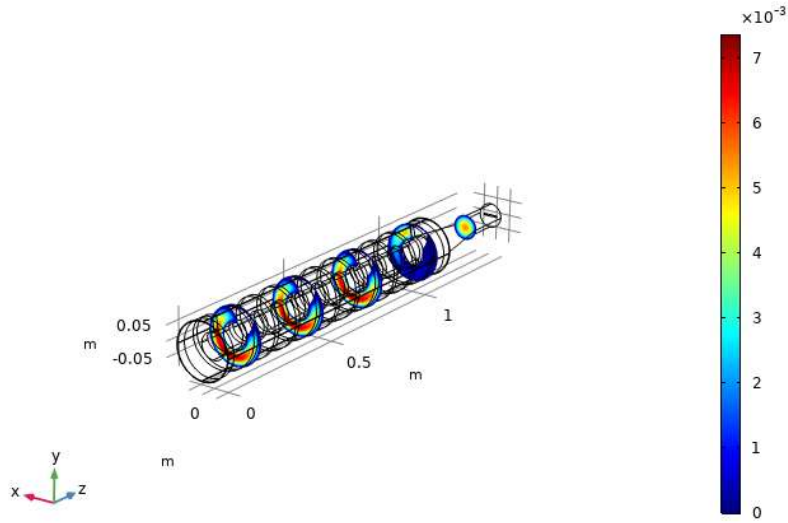


Figure 7: xy Plane of Velocity Field

The yz plane of the velocity field was also modeled. Similar to the xy plane, velocity remains uniform until the transition zone, where it drops suddenly. It increases again in the die and begins to decrease upon die exit. As with the xy plan, decreases in velocity are observed as the screw and barrel walls are approached.

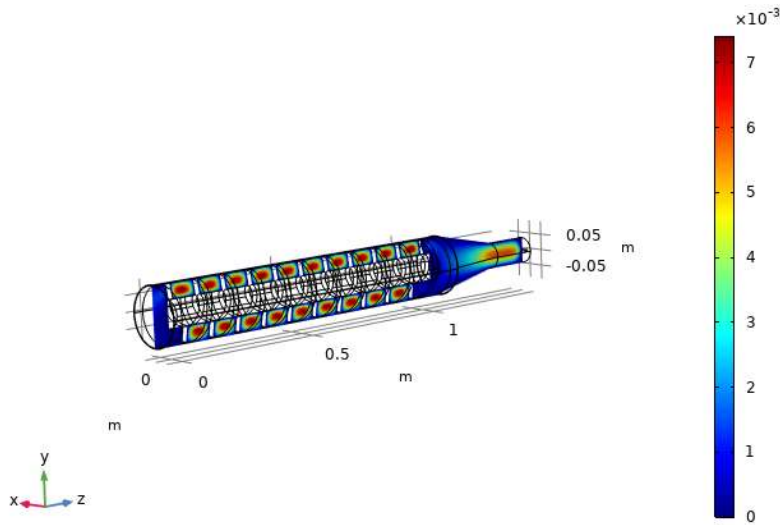


Figure 8: yz Plane of Velocity Field

Discussion

As indicated in the results section, a pressure gradient develops across the extruder field. With a 20 MPa pressure force applied at the entrance boundary of the extruder model, one can see a clear decrease in pressure as the melt moves through the melting zone and an even further decrease in pressure as it moves through the die out of the extruder. Based on the report's model, a pressure gradient would develop along the barrel and through the die, ultimately leading to the die's expansion. This is in alignment with the observed experimental results. However, there would be a higher pressure force acting near the interior of the melt, which is associated with a higher velocity field observed there. This was not in alignment with the experimental results. One possible reason for this outcome is the lack of spatial terms in the proposed momentum equation used in the experiments.

The temperature field in the model remains relatively constant through the barrel. There is a slight drop in temperature at the onset of the melting zone, at which point the temperature remains steady until it reaches the die. At the die, a slight increase in temperature is seen. Based on the model in the report, the melt is predicted to cool from the outside. However, heat is released through convection and evaporation at the melt's surface near the extruder barrel walls, so the predicted lower temperature at the outer edges of the melt does not agree with experimental results. This can be attributed to the experimental model's input parameters, which used a constant radius with no expansion effects and no spatial terms incorporated into the temperature gradient. At the onset of the transition zone, the report's model predicts a decrease in temperature due to the onset of expansion. In addition, the latent heat of vaporization of the bubbles formed would decrease temperature. This is corroborated by experimental results. However, the report's model does not predict the slight increase upon exit from the die observed in the experimental results.

The yz temperature plane remains fairly steady along the extruder path. No significant changes in the temperature field are observed until the die section, where a very slight increase is observed.

The xy velocity plane exhibits a gradient along the axis of the screw at various points along the extruder barrel. Velocity is shown to be at its highest in the interior sections of the melt, with a negative velocity gradient seen as the barrel walls are approached. At the onset of the transition

zone to the die, the lowest velocity is observed, upon which an increase in velocity profile is seen in the interior of the die. The die velocity profile again exhibits the highest velocity in the melt interior. Based on the proposed model in the report, velocity is predicted to be higher at the center of the melt at any given point along the barrel, with velocity dropping as one approaches both the screw and the barrel walls. This is in agreement with the experimental results. In addition, the report model predicts velocity dropping as the melt enters the transition zone, as the radius of the melt decreases and pressure drops. Lastly, velocity increases upon exit before dropping due to increased viscosity during expansion. This is also in line with experimental observations.

The yz velocity plane exhibits a similar trend to the xy velocity plane. Velocity is low at the onset of the extruder barrel, and an increase is observed initially, at which point velocity remains steady at this elevated level through the barrel. At the onset of the die transition zone, a sharp decrease in velocity is observed, followed by an increase as the melt exits the die. The interior of the melt exhibits higher velocities throughout the system.

Conclusion

The research field of extrusion cooking for plant-based meats remains an underutilized field of study, although that is rapidly changing. As more money and resources are invested into this field, research initiatives will advance and lead to a better understanding of heat, mass and momentum transport phenomena. This will result in more complex and accurate mathematical models being developed. This report identified and assessed the most important parameters affecting plant-based meat products in extrusion cooking to create a mathematical model to mimic real-time behaviors. The effects of modulating each of these parameters and their impact on overall product quality were explained. Comparison to experimental results was explained. Computational models for plant-based meat extrusion cooking are very complex. A slight change in one parameter can affect multiple other parameters and those relationships need to be fully explored and understood. Further research into these isolated parameters and their effects is needed to advance this research in the near future.

References

1. [Martinez et al.](#) Technological Properties of Chickpea (*Cicer Arietinum*): Production of Snacks and Health Benefits Related to Type-2 Diabetes. *Comprehensive Reviews in Food Science and Food Safety*, (2021), 20 (4), pp. 3762-3787.
2. [Angelova et al.](#) Effect of Selected Parameters on Sectional Expansion Index and Bulk Density During the Extrusion of Chickpea Instant Semolina. *Technology and Safety of Food Products*. (2021), 15 (2) pp. 79-84.
3. [Meng et al.](#) Effects of Extrusion Conditions on System Parameters and Physical Properties of a Chickpea Flour-based Snack. *Food Research International*. (2010), 43 (2), pp. 650-658.
4. [Guldiken et al.](#) Effect of Extrusion Conditions on the Physical Properties of Desi Chickpea-barley Extrudates and Quality Attributes of their Resulting Flours. *Journal of Texture Studies*. (2020), 51 (2), pp. 300-307
5. [Manepalli et al.](#) Stochastic Modeling of Expansion of Starchy Melts During Extrusion. *Journal of Food Engineering*. (2019), 245, pp. 57-64.
6. [Webb et al.](#) Role of Chickpea Flour in Texturization of Extruded Pea Protein. *Journal of Food Science*. (2020), 85 (12), pp. 4180-4187.
7. [Gu et al.](#) *Food Extrusion Processing: An Overview*. Washington State University. (2017).
8. [Kumar et al.](#) *Extrusion of Foods. Mathematical Modeling of Food Processing*. CRC Press. (2010), pp. 809-820.

9. [Ferretti, Gino and Roberto Montanari](#). A Finite Difference Method for the Prediction of Velocity Field in Extrusion Process. *Journal of Food Engineering*. (2007), 83 (1), pp. 84-92.
10. [Dhanasekharan, Kumar and Jozef Kokini](#). Design and Scaling of Wheat Dough Extrusion by Numerical Simulation of Flow and Heat Transfer. *Journal of Food Engineering*. (2003), 60 (4), pp. 421-430.
11. [Wang et al.](#) Modeling of Transport Phenomena and Melting Kinetics of Starch in a Co-Rotating Twin-Screw Extruder. *Advances in Polymer Technology*. (2006), 25 (1), pp. 22-40.
12. [Manepalli et al.](#) Mathematical Modeling of Flow Behavior and Cell Structure Formation During Extrusion of Starchy Melts. *Journal of Food Engineering*. (2017), 198, pp. 7-16.
13. [Kristiawan et al.](#) Extrusion Simulation for the Design of Cereal and Legume Foods. *Foods*. (2022), 11 (12), 1780.
14. [Ma et al.](#) Modelling and Comparison of Wheat Flour Extrusion Cooking Behaviors in Two Different Twin-Screw Extrusion Systems. *Food and Bioprocess Technology*. (2018), 11 (7), pp. 1381-1392.
15. [Cheng, Hongyuan and Alan Friis](#). Modeling Extrudate Expansion in a Twin-screw Food Extrusion Cooking Process Through Dimensional Analysis Methodology. *Food and Bioproducts Engineering*. (2010), 88 (2-3), pp. 188-194.
16. [Wang et al.](#) Modeling of Bubble Growth Dynamics and Nonisothermal Expansion in Starch Based Foams During Extrusion. *Advances in Polymer Technology*. (2005), 24 (1), pp. 29-45.

17. [Kristiawan et al.](#) Modeling of Starchy Melts Expansion by Extrusion. Trends in Science and Food Technology. (2016), 48, pp. 13-26.
18. [Singha et al.](#) Influence of Processing Conditions on Apparent Viscosity and System Parameters During Extrusion of Distiller's Dried Grains-based Snacks. Food Science and Nutrition. (2018), 6 (1), pp. 101-110.
19. [Ditudompo, Srivikorn and Pawan Takhar.](#) Hybrid Mixture Theory Based Modeling of Transport Mechanisms and Expansion-Thermomechanics of Starch During Extrusion. AIChE Journal. (2015), 61 (12), pp. 4517-4532.
20. [Wilczynski et al.](#) Fundamentals of Global Modeling for Polymer Extrusion. Polymers. (2019), 11 (12), 2106.
21. [Pricci et al.](#) Analytical and Numerical Models of Thermoplastics: A Review Aimed to Pellet Extrusion-Based Additive Manufacturing. Polymers. (2021), 13 (18), 3160.
22. [Hyvarinen et al.](#) The Modeling of Extrusion Processes for Polymers – A Review. Polymers, (2020), 12 (6), 1306.
23. [Wilczynski et al.](#) Computer Modeling for Single-Screw Extrusion of Wood-Plastic Composites. Polymers, (2018), 10 (3), 274.
24. [Lewandowski, Adrian and Krzysztof Wilczynski.](#) Modeling of Twin Screw Extrusion of Polymeric Materials. Polymers. (2022), 14 (2).
25. [McGuire et al.](#) Food Powder Flow in Extrusion: Role of Particle Size and Composition. Processes. (2022), 10 (1), 178.

26. [Carr, Elliot and Nathan March](#). Semi-analytical Solution of Multilayer Diffusion Problems with Time-varying Boundary Conditions and General Interface Conditions. *Applied Mathematics and Computation*. (2019), 333, pp. 286-303.
27. [Xia et al.](#) Effects of Food Components and Processing Parameters on Plant-based Meat Texture Formation and Evaluation Methods. *Journal of Texture Studies*. (2022).
28. [Wang et al.](#) Flavor Challenges in Extruded Plant-based Meat Alternatives: A Review. *Comprehensive Reviews in Food Science and Food Safety*. (2022), 21 (3), pp. 2898-2929.
29. [Fu et al.](#) Structure Analysis and Quality Evaluation of Plant-based Meat Analogs. *Journal of Texture Studies*. (2022).
30. [Leonard et al.](#) Application of Extrusion Technology in Plant Food Processing Byproducts: An Overview. *Comprehensive Reviews in Food Science and Food Safety*. (2020), 19 (1), pp. 218-246.
31. [Ajita, Tiwari and Jha S. K.](#) Extrusion Cooking Technology: Principal Mechanism and Effect on Direct Expanded Snacks – An Overview. *International Journal of Food Studies*. (2017), 6 (1), pp. 113-128.
32. [Zhang et al.](#) High Moisture Extruded Protein Fiber Formation Toward Plant-based Meat Substitutes Applications: Science, Technology and Prospect. *Trends in Food Science and Technology*. (2022), 128, pp. 202-216.
33. [Wittek et al.](#) Morphology Development and Flow Characteristics During High Moisture Extrusion of a Plant-based Meat Analogue. *Foods*. (2021), 10 (8), 1753.
34. [Frame, N.D.](#) *The Technology of Extrusion Cooking*. Springer. (1995), pp. 88-89.

35. [Aguilo-Aguayo et al.](#) Emerging Thermal Processes in the Food Industry. Woodhead Publishing. Emerging Thermal Processes in the Food Industry. (2023), pp. 1-29.
36. [Hilliou, Loic and Jose A Covas.](#) In-process Rheological Monitoring of Extrusion-based Polymer Processes. Polymer International. (2021), 70 (1), pp. 24-33.
37. [Estrada, Omar and Farid Chejne Janna.](#) A Novel Melting Model for Polymer Extrusion: Mechanically Induced Transition Layer Removal. Polymer Engineering and Science. (2022), 62 (1), pp. 3290-3309.
38. [Formela et al.](#) Reactive Extrusion of Bio-based Polymer Blends and Composites – Current Trends and Future Developments. eXPRESS Polymer Letters. (2018), 12 (1), pp. 24-57.
39. [Ek, Pichmony and Girish M. Ganjyal.](#) Extrusion Cooking, Cereal Grain Processing. Elsevier. (2020), 2, pp. 1-28.
40. [Toukhtarian et al.](#) Modeling Polymer Extrusion with Varying Die Gap using Arbitrary Lagrangian Eulerian (ALE) Method. Physics of Fluids. (2018), 30 (9).
41. [Wilczynski et al.](#) Rheological Basics for Modeling of Extrusion Process of Wood Polymer Composites. Polymers. (2021), 13 (4), 622.
42. [Amangeldi et al.](#) Numerical Modeling of Thermal Flows in Entrance Channels for Polymer Extrusion: A Parametric Study. Processes. (2020). 8 (1), 1256.
43. [Zairi et al.](#) Steady Plastic Flow of a Polymer During Equal Channel Angular Extrusion Process: Experiments and Numerical Modeling. Polymer Engineering and Science. (2008), 48 (5), pp. 1015-1021.

44. [Hosseini et al.](#) Modeling of Extrusion Process and Application of Taguchi Method and ANOVA Analysis for Optimization the Parameters. *Mechanika*. (2012), 18 (3), pp. 301-305.
45. [Abeykoon et al.](#) Dynamic Modeling of Die Melt Temperature Profile in Polymer Extrusion: Effects of Process Settings, Screw Geometry and Material. *Applied Mathematical Modeling*. (2014), 38 (4), pp. 1224-1236.
46. [Mu et al.](#) Modeling and Simulation of Polymer Melts Flow in the Extrusion Process of Plastic Profile with Metal Insert. *The International Journal of Advanced Manufacturing Technology*. (2013), 67 (1-4), pp. 629-646.
47. [Wilczynski et al.](#) A Computer Model for Starve-fed Single-screw Extrusion of Polymer Blends. *Advances in Polymer Technology*. (2018), 37 (6), pp. 2142-2151.
48. [Kadyirov et al.](#) Numerical Simulation of Polymer Solutions in a Single-Screw Extruder. *Applied Sciences*. (2019), 9 (24), 5423.
49. [Roland, Wolfgang and Jurgen Miethlinger](#). Heuristic Analysis of Viscous Dissipation in Single-Screw Extrusion. *Polymer Engineering and Science*. (2018), 58 (11), pp. 2055-2070.
50. [Hammer et al.](#) Experimental Validation of Non-Newtonian Stratified Co-Extrusion Prediction Models Using a Digital Process Twin. *Polymer Engineering and Science*. (2022), 62 (12), pp. 3902-3922.
51. [Marschik et al.](#) Melt Conveying in Single-Screw Extruders: Modeling and Simulation. *Polymers*. (2022), 15 (5), 875.

52. [Eitzlmyer et al.](#) Experimental Characterization and Modeling of Twin-Screw Extruder Elements for Pharmaceutical Hot Melt Extrusion. *AIChE Journal*. (2013), 59 (11), pp. 4440-4450.

53. [Good Food Institute](#). Deep Dive: Plant-based Meat End Product Formulation and Manufacturing. Good Food Institute. (2023).

54. [J. Lunn and E. Theobald](#). The Health Effects of Dietary Unsaturated Fatty Acids. *Nutrition Bulletin*. (2006), 31 (3), pp. 178-224.

